Geosci. Model Dev. Discuss., 7, 8565–8647, 2014
www.geosci-model-dev-discuss.net/7/8565/2014/
doi:10.5194/gmdd-7-8565-2014

Geoscientific Model Development Discussions

A vertically discretised canopy description for ORCHIDEE (SVN r2290) and the modifications to the energy, water and carbon fluxes

K. Naudts[1], J. Ryder[1], M. J. McGrath[1], J. Otto[1,10], Y. Chen[1], A. Valade[1], V. Bellasen[2], G. Berhongaray[3], G. Bönisch[4], M. Campioli[3], J. Ghattas[1], T. De Groote[3,11], V. Haverd[5], J. Kattge[4], N. MacBean[1], F. Maignan[1], P. Merilä[6], J. Penuelas[7,12], P. Peylin[1], B. Pinty[8], H. Pretzsch[9], E. D. Schulze[4], D. Solyga[1,13], N. Vuichard[1], Y. Yan[3], and S. Luyssaert[1]

[1]LSCE, IPSL, CEA-CNRS-UVSQ, 91191 Gif-sur-Yvette, France
[2]UMR CESAER, INRA, 21079 Dijon, France
[3]Department of Biology, University of Antwerp, 2610 Wilrijk, Belgium
[4]MPI-Biogeochemistry, Jena, Germany
[5]CSIRO-Ocean and Atmosphere Flagship, 2600 Canberra, Australia
[6]METLA, Oulu, Finland
[7]Global Ecology Unit CREAF-CSIC-UAB, Cerdanyola del Valles, Spain
[8]European Commission, Joint Research Centre, Ispra, Italy

[9]Center of Life and Food Sciences, TUM, Munich, Germany
[10]Helmholtz-Zentrum Geesthacht, Climate Service Center 2.0, Hamburg, Germany
[11]VITO, 2400 Mol, Belgium
[12]CSIC, Barcelona, Spain
[13]CGG, 91341 Massy, France

Received: 29 October 2014 – Accepted: 5 November 2014 – Published: 5 December 2014

Correspondence to: K. Naudts (kim.naudts@lsce.ipsl.fr)

Published by Copernicus Publications on behalf of the European Geosciences Union.

Abstract

Since 70 % of global forests are managed and forests impact the global carbon cycle and the energy exchange with the overlying atmosphere, forest management has the potential to mitigate climate change. Yet, none of the land surface models used in Earth system models, and therefore none of today's predictions of future climate, account for the interactions between climate and forest management. We addressed this gap in modelling capability by developing and parametrizing a version of the land surface model ORCHIDEE to simulate the biogeochemical and biophysical effects of forest management. The most significant changes between the new branch called ORCHIDEE-CAN (SVN r2290) and the trunk version of ORCHIDEE (SVN r2243) are the allometric-based allocation of carbon to leaf, root, wood, fruit and reserve pools; the transmittance, absorbance and reflectance of radiation within the canopy; and the vertical discretisation of the energy budget calculations. In addition, conceptual changes towards a better process representation occurred for the interaction of radiation with snow, the hydraulic architecture of plants, the representation of forest management and a numerical solution for the photosynthesis formalism of Farquhar, von Caemmerer and Berry. For consistency reasons, these changes were extensively linked throughout the code. Parametrization was revisited after introducing twelve new parameter sets that represent specific tree species or genera rather than a group of unrelated species, as is the case in widely used plant functional types. Performance of the new model was compared against the trunk and validated against independent spatially explicit data for basal area, tree height, canopy strucure, GPP, albedo and evapotranspiration over Europe. For all tested variables ORCHIDEE-CAN outperformed the trunk regarding its ability to reproduce large-scale spatial patterns as well as their inter-annual variability over Europe. Depending on the data stream, ORCHIDEE-CAN had a 67 to 92 % chance to reproduce the spatial and temporal variability of the validation data.

1 Introduction

Forests play a particularly important role in the global carbon cycle. Forests store almost 50 % of the terrestrial organic carbon and 90 % of vegetation biomass (Dixon et al., 1994). Globally, 70 % of the forest is managed and the importance of management is still increasing both in relative and absolute terms. In densely populated regions, such as Europe, almost all forest is intensively managed by humans. Recently, forest management has become a top priority on the agenda of political negotiations to mitigate climate change. Because forest plantations may remove CO_2 from the atmosphere, harvested timber is a substitute for fossil fuel if used for energy production. Forest management thus has great potential for mitigating climate change, which was recognized in the United Nations Framework Convention on Climate Change and the Kyoto Protocol.

Forests not only influence the global carbon cycle, they also dramatically affect the water vapour and energy fluxes exchanged with the overlying atmosphere. It has been shown, for example, that the evapotranspiration of young plantations can be so great that the streamflow of neighbouring creeks is reduced by 50 % (Jackson et al., 2005). Modelling studies on the impact of forest plantations in regions that are snow-covered in winter suggest that because of their darkness (the so-called albedo), forest could increase regional temperature by up to four degrees (Betts, 2000; Bala et al., 2007; Davin et al., 2007; Zhao and Jackson, 2014). Management-related changes in the albedo, energy balance and water cycle of forests (Amiro et al., 2006a, b) are of the same magnitude as the differences between forests, grasslands and croplands (Luyssaert et al., 2014). Moreover, changes in the water vapour and the energy exchange may offset the cooling effect obtained by managing forests as stronger sinks for atmospheric CO_2 (Pielke et al., 2002). Despite the key implications of forest management on the carbon-energy-water exchange there have been no integrated studies on the effects of forest management on the Earth's climate.

Earth system models are the most advanced tools to predict future climate (Bonan, 2008). These models represent the interactions between the atmosphere and the surface beneath, with the surface formalized as a combination of open oceans, sea ice and land. For land, five classes are distinguished: glacier, lake, wetland, urban and vegetated. Vegetated surfaces are sub-divided in patches of different plant functional types. ORCHIDEE is the land surface component of the IPSL (Institut Pierre Simon Laplace) Earth System Model. Hence, by design, the ORCHIDEE model can be run coupled to the global circulation model LMDz. In this coupled set-up, the atmospheric conditions affect the land surface and the land surface, in turn, affects the atmospheric conditions. Coupled land-atmosphere models thus offer the possibility to quantify both the climatic effects of changes in the land surface and the effects of climate change on the land surface. The most advanced land-surface models used, for instance, in Earth System Models to predict climate changes (see the recent CMIP5 exercise), account for changes in vegetation cover but consider forests to be mature and ageless, e.g., JSBACH (Reick et al., 2013), CLM (Stöckli et al., 2008), MOSES (Cox et al., 1999), ORCHIDEE (Krinner et al., 2005) and LPJ-DVGM (Bonan et al., 2003). At present, none of the predictions of future climate thus account for the essential interactions between forest management and climate. This gap in modelling capability provides the motivation for further development of the land-surface model ORCHIDEE to realistically simulate both the biophysical and biogeochemical effects of forest management on the climate. The ORCHIDEE-CAN (short for ORCHIDEE-CANOPY) branch of the land surface model was specifically developed to quantify the climatic effects of forest management.

2 Model overview

2.1 The Starting point: ORCHIDEE SVN r1170

The land surface model used for this study, ORCHIDEE, is based on two different modules (Krinner et al., 2005, their Fig. 2). The first module describes the fast processes such as the soil water budget and the exchanges of energy, water and CO_2 through photosynthesis between the atmosphere and the biosphere (Ducoudré et al., 1993; de Rosnay and Polcher, 1998). The second module simulates the carbon dynamics of the terrestrial biosphere and essentially represents processes as maintenance and growth respiration, carbon allocation, litter decomposition, soil carbon dynamics and phenology (Viovy and de Noblet-Ducoudré, 1997). The trunk version of ORCHIDEE describes global vegetation by 13 metaclasses (MTC) with a specific parameter set (one for bare soil, eight for forests, two for grasslands and two for croplands). Each MTC can be divided into a user-defined number of PFTs which can be characterised by at least one parameter value that differs from the parameter settings of the MTC. Parameters that are not given at the PFT-level are assigned the default value for the MTC to which the PFT belongs. By default none of the parameters are specified at the PFT-level, hence, MTCs and PFTs are the same for the standard ORCHIDEE trunk version. A concise description of the main processes in the ORCHIDEE-trunk version and a short motivation to change these modules in ORCHIDEE-CAN is given in Table 1.

Before running simulations, it is necessary to bring the soil carbon pools into equilibrium due to their slow fill rates, an approach known as model spin-up (Thornton and Rosenbloom, 2005; Xia et al., 2012). For a long time, spin-ups have been performed by brute force, i.e., running the model iteratively over a sufficiently long period which allows even the slowest carbon pool to reach equilibrium. This native approach is reliable but slow (in the case of ORCHIDEE it takes 3000 years) and thus comes with a large computational demand, often exceeding the computational cost of the simulation itself. Alternative spin-up methods calling only parts of the model, e.g., subsequent cycles of 10 years of only photosynthesis followed by 100 year cycles of only soil pro-

cesses, have been used for ORCHIDEE to reduce the computational cost in the past. These approaches, however, tend to lead to instabilities in litter and carbon pools. In recent years, semi-analytical methods have been proposed as a cost-effective solution to the spin-up issue (Martin et al., 2007; Lardy et al., 2011; Xia et al., 2012). A matrix-sequence method has been implemented in ORCHIDEE following the approach used by the PaSim model (Lardy et al., 2011). The semi-analytical spin-up implemented in ORCHIDEE relies on algebraic methods to solve a linear system of equations describing the seven carbon pools separately for each PFT. Convergence of the method and thus equilibrium of the carbon pools is assumed to be reached when the variation of the passive carbon pool (which is the slowest) drops below a predefined threshold. The net biome production (NBP) is used as a second diagnostic criterion to confirm convergence. In order to optimize computing resources, the semi-analytical spin-up will stop before the end of the run once the convergence criteria are met. ORCHIDEE's implementation of the semi-analytical spin-up has been validated at regional and global scales against a native spin-up, and has been found to converge 12 to 20 times faster. The largest gains were realised in the tropics and the smallest gains in boreal climate.

2.2 Modifications between ORCHIDEE SVN r2243 and ORCHIDEE-CAN SVN r2290

One major overarching change in the ORCHIDEE-CAN branch is the increase of internal consistency within the model by adding connections between the different processes (see Fig. 1, red arrows). A more specific novelty is the introduction of circumference classes within forest PFTs, based on the work of Bellassen et al. (2010). For the temperate and boreal zone, tree height and crown diameter are calculated from allometric relationships of tree diameter that were parametrized based on the French, Spanish, Swedish and German forest inventory data and the observational data from (Pretzsch, 2009). The circumference classes thus allow calculation of the social position of trees within the canopy which justifies applying an intra-tree competition rule (Deleuze et al., 2004) to account for the fact that trees with a dominant position in

the canopy are more likely to intercept light than suppressed trees, and, therefore, contribute more to the stand level photosynthesis and biomass growth. To respect the competition rule of Deleuze et al. (2004), a new allocation scheme was developed based on the pipe model theory (Shinozaki et al., 1964) and its implementation by Sitch et al. (2003). The scheme allocates carbon to different biomass pools (leaves, fine roots, and sapwood) while respecting the differences in longevity and hydraulic conductivity between the pools. In addition to the biomass of the different pools, LAI, crown volume, crown density, stem diameter, stem height and stand density are calculated and now depend on accumulated growth. The new scheme allows for the removal of the parameter that caps the maximum LAI (see Table 1).

The calculation of tree dimensions (e.g., sapwood area and tree height) that respect the pipe theory supports making use of the hydraulic architecture of plants to calculate the plant water supply (Fig. 1, arrow 1), which is the amount of water a plant can transport from the soil to its stomata. The representation of the plant hydraulic architecture is based on the scheme of Hickler et al. (2006). The water supply is calculated as the ratio of the pressure difference between soil and leaves, and the total hydraulic resistance of the roots, leaves and sapwood, where the latter is increased when cavitation occurs. Species-specific parameter values were compiled from the literature. As the scheme makes use of the soil water potential, it requires the use of the 11 layer hydrology scheme of de Rosnay (2002) (see Table 1). When transpiration based on energy supply exceeds transpiration based on the water supply, the latter restricts stomatal conductance directly, which is a physiologically more realistic representation of drought stress than the reduction of k_{Vcmax} done in the trunk (Flexas et al., 2006). In line with this approach, the drought stress factor used to trigger phenology and senescence is now calculated as the ratio between the transpiration based on water supply and transpiration based on atmospheric demand (Fig. 1, arrow 2).

The new allocation scheme also drastically changed the way forests are represented in the ORCHIDEE-CAN branch. Although the exact location of the canopies in the stand is not known, individual tree canopies are now spherical elements with their

horizontal location following a Poisson distribution across the stand. Each PFT contains a user-defined number of model trees, each one corresponding to a circumference class. Model trees are replicated to give realistic stand densities. Following tree growth, canopy dimensions and stand density are updated (Fig. 1, arrow 3). This formulation results in a dynamic canopy structure that is exploited in other parts of the model, i.e., precipitation interception, transpiration, energy budget calculations, albedo (Fig. 1, arrow 4) and absorbed light for photosynthesis (Fig. 1, arrow 5). In the trunk version these processes are driven by the big-leaf canopy assumption. The introduction of an explicit canopy structure is thought to be a key development with respect to the objectives of the ORCHIDEE-CAN branch, i.e., quantifying the biogeochemical and biophysical effects of forest management on atmospheric climate.

The radiation transfer scheme at the land surface benefits from the introduction of canopy structure. The trunk version of ORCHIDEE prescribes the vegetation albedo solely as a function of LAI. In the ORCHIDEE-CAN branch each tree canopy is assumed to be composed of uniformly distributed single scatterers. Following the assumption of a Poisson distribution of the trees on the land surface, the model of Haverd et al. (2012) calculates the transmission probability of light to any given vertical point in the forest. This transmission probability is then used to calculate an effective LAI, which is a statistical description of the vertical distribution of leaf mass that accounts for stand density and horizontal tree distribution. The complexity and computational costs are largely reduced by using the effective LAI in combination with the 1-D two stream radiation transfer model of Pinty et al. (2006) rather than resolving a full 3-D canopy model. By using the effective LAI, the 1-D model reproduces the radiative fluxes of the 3-D model. The approach of the two stream radiation transfer model was extended for a multi-layer canopy (McGrath et al., 2014). The scattering parameters and the background albedo (i.e. the albedo of the surface below the dominant tree canopy) for the two stream radiation transfer model were extracted from the Joint Research Centre Two-stream Inversion Package (JRC-TIP) remote sensing product (see Sect. 4.7). This approach produces fluxes of the light absorbed, transmitted, and re-

flected by the canopy at vertically discretized levels, which are then used for the energy budget (Fig. 1, arrow 6) and photosynthesis calculations (Fig. 1, arrow 5).

The canopy radiative transfer scheme of (Pinty et al., 2006) separates the calculation of the fluxes resulting from downwelling direct and diffuse light, with different scattering parameters available for near-infrared (NIR) and visible (VIS) light sources. The snow albedo scheme in the trunk does not distinguish between these two shortwave bands. Therefore, the snow albedo scheme of the Biosphere-Atmosphere Transfer Scheme (BATS) for the Community Climate Model (Dickinson et al., 1986) was incorporated into the ORCHIDEE-CAN branch, since it distinguishes between the NIR and VIS radiation. The radiation scheme of Pinty et al. (2006) requires snow to be put on the soil below the tree canopy instead of on the canopy itself. The calculation of the snow coverage of a PFT therefore had to be revised according to the scheme of Yang et al. (1997), which allows for snow to completely cover the ground at depths greater than 0.2 m. The parameter values of Yang et al. (1997) were used in the ORCHIDEE-CAN branch.

The ORCHIDEE-CAN branch differs from any other land surface model by the inclusion of a newly developed multi-layer energy budget. There are now subcanopy wind, temperature, humidity, longwave radiation and aerodynamic resistance profiles, in addition to a check of energy closure at all levels. The energy budget represents an implementation of some of the characteristics of detailed single site, iterative canopy models (e.g., Baldocchi, 1988; Ogee et al., 2003) within a system that is coupled implicitly to the atmosphere. Contrary to the trunk version of ORCHIDEE (see Table 1), the new approach generates a leaf temperature, using the same vegetation and radiation profile generated in the radiation scheme above, which will be fully available when parametrisation of the scheme has been completed across test sites corresponding to the species within the model. As with the trunk version, the new energy budget is calculated implicitly (Polcher et al., 1998; Best et al., 2004), so as to allow for, given the 15 min time-step, a computationally efficient and stable coupling to the atmospheric model LMDz. Parameters were derived by optimizing the model against observations from short-term field campaigns. The new scheme may also be reduced to the existing

single layer case so as to provide a means of comparison and compatibility with the trunk version of ORCHIDEE.

The combined use of the new energy budget and the hydraulic architecture of plants required changes to the calculation of the stomatal conductance and photosynthesis (Fig. 1, arrow 7). When water supply limits transpiration, stomatal conductance is reduced and photosynthesis needs to be recalculated. Given that photosynthesis is among the computational bottlenecks of the model, the semi-analytical procedure as available in previous trunk versions is replaced by an adjusted implementation of the analytical photosynthesis scheme of Yin and Struik (2009), which is also implemented in the latest ORCHIDEE-trunk version. In addition to an analytical solution for photosynthesis the scheme includes a modified Arrhenius function for the temperature dependence that accounts for a decrease of k_{Vcmax} and k_{Jmax} at high temperatures and a temperature dependent $k_{\mathrm{Jmax/Vcmax}}$ ratio (Kattge and Knorr, 2007). The temperature response of k_{Vcmax} and k_{Jmax} was parametrized with values from reanalysed data in literature (Kattge and Knorr, 2007), whereas k_{Vcmax} and k_{Jmax} at a reference temperature of 25 °C were derived from observed species-specific values in the TRY database (Kattge et al., 2011). As the amount of absorbed light varies with height (or canopy depth), the absorbed light computed from the albedo routines is now directly used in the photosynthesis scheme resulting in full consistency between the top of the canopy albedo and absorption. This new approach replaces the old scheme which used multiple levels based on the leaf area index, not the physical height.

ORCHIDEE-CAN incorporates a systematic mass balance closure for carbon cycling to assure that carbon is not getting created or destroyed during the simulation. Hence, budget closure is now consistently checked for water, carbon and energy throughout the model.

The trunk uses 13 plant functional types (PFT) to represent vegetation globally: one PFT for bare soil, eight for forests, two for grasslands, and two for croplands. The ORCHIDEE-CAN branch makes use of the externalization of the PFT-depedent parameters by adding 12 parameter sets that represent the main European tree species.

Species parameters were extracted from a wide range of sources including original observations, large databases, primary research and remote sensing products (see Sect. 4). The use of age classes is introduced through externalization of the PFT parameters as well. Age classes are used during land cover change and forest management to simulate the regrowth of a forest. Following a land cover change, biomass and soil carbon pools (but not soil water columns) are mixed. The number of age classes is user defined. Contrary to typical age classes, the boundaries are determined by the tree diameter rather than the age of the trees.

Finally, the forest management strategies in the ORCHIDEE-CAN branch were refined from the original forest management branch (Bellassen et al., 2010). Self-thinning was activated for all forests regardless of human management, contrary to the original FM branch. The new default management strategy thus has no human intervention but includes self-thinning, which replaces the fixed 40 year turnover time for woody biomass. Three management strategies with human intervention have been implemented: (1) "High stands", in which human intervention is restricted to thinning operations based on stand density and diameter, with occasional clearcuts. Aboveground stems are harvested during operations, while branches and belowground biomass are left to litter. (2) "Coppices" involve two kinds of cuts. The first coppice cut is based on stem diameter and the aboveground woody biomass is harvested whereas the belowground biomass is left living. From this belowground biomass new shoots sprout, which increases the number of aboveground stems. In subsequent cuts the amount of shoots is not increased, although all aboveground wood biomass is still harvested. (3) "Short rotation coppices", where rotation periods are based on age and are generally very short (3–6 years). The different management strategies can occur with or without litter raking, which reduces the litter pools and has a longterm effect on soil carbon (Gimmi et al., 2012). All management types are parametrized based on forest inventory data, yield tables and guidelines for forest management. The inclusion of forest management resulted in two additional carbon pools, branches and coarse roots (i.e., abovegound and belowground woody biomass) and therefore required an extension to the semi-

analytical spin-up method (see Sect. 2.1). The semi-analytical spin-up is now run for nine C pools.

3 Description of the developments

3.1 Allocation

Following bud burst, photosynthesis produces carbon that is added to the labile carbon pool. Labile carbon is used to sustain the maintenance respiration flux (F_{rm}), which is the carbon cost to keep existing tissue alive (Amthor, 1984). Maintenance respiration for the whole plant is calculated by summing maintenance respiration of the different plant compartments, which is a function of the nitrogen concentration of the tissue (Zaehle and Friend, 2010, their Eqs. 6 and 7) and subtracted from the whole-plant labile pool (up to a maximum of 80 % of the labile pool).

The remaining labile carbon pool is split into an active and none-active pool. The size of the active pool is calculated as a function of plant phenology and temperature and was formalized following Ryan (1991); Sitch et al. (2003); Zaehle and Friend (2010). The remaining non-active pool is used to restore the labile and carbohydrate reserves pools according to the rules proposed in Zaehle and Friend (2010). The labile pool is limited to 1 % of the plant biomass or 10 times the actual daily photosynthesis. Any excess carbon is transferred to the non-respiring carbohydrate reserve pool. The carbohydrate reserve pool is capped to reflect limited starch accumulation in plants, but carbon can move freely between the two reserve pools. After accounting for growth respiration (F_{rg}), i.e., the cost for producing new tissue excluding the carbon required to build the tissue itself (Amthor, 1984), the total allocatable C used for plant growth is obtained (M_{totinc}).

New biomass is allocated to leaves, roots, sapwood, heartwood, and fruits. Allocation to leaves, roots and wood respects the pipe model theory (Shinozaki et al., 1964) and thus assumes that producing one unit of leaf mass requires a proportional amount

of sapwood to transport water from the roots to the leaves as well as a proportional fraction of roots to take up the water from the soil. The scaling parameter between leaf and sapwood mass is derived from:

$$d_l = k_{ls} \times m_w \times d_s \quad (1)$$

where d_l is the one-sided leaf area of an individual plant, d_s is the sapwood area of an individual plant, k_{ls} a parameter linking leaf area to sapwood area and, m_w is the water stress as defined in Sect. 3.2. Alternatively, leaf area can be written as a function of leaf mass (M_l) and the specific leaf area (k_{sla}):

$$d_l = M_l \times k_{sla} \quad (2)$$

Sapwood mass M_s can be calculated from the sapwood area d_s as follows:

$$M_s = d_s \times d_h \times k_{\rho s} \quad (3)$$

where d_h is the tree height and $k_{\rho s}$ is the sapwood density. Following substitution of Eqs. (2) and (3) into Eq. (1), leaf mass can be written as a function of sapwood mass:

$$M_l = (M_s \times f_{KF}) / d_h \quad (4)$$

where,

$$f_{KF} = (k_{ls} \times m_w) / (k_{sla} \times k_{\rho s}) \quad (5)$$

where, k_{ls} is calculated as a function of the gap fraction as supported by site-level observations (Simonin et al., 2006):

$$k_{ls} = k_{lsmin} + f_{Pgap,trees} \times (k_{lsmax} - k_{lsmin}) \quad (6)$$

k_{lsmin} is the minimum observed leaf area to sapwood area ratio, k_{lsmax} is the maximum observed leaf area to sapwood area ratio and $f_{Pgap,trees}$ is the actual gap fraction. By

using the gap fraction as a control of k_{ls} more carbon will be allocated to the leaves until canopy closure is reached.

Following Magnani et al. (2000), sapwood mass and root mass (M_r) are related as follows:

$$M_s = k_{sar} \times d_h \times M_r \quad (7)$$

where the parameter k_{sar} is calculated according to Magnani et al. (their Eq. 17):

$$k_{sar} = \sqrt{(k_{rcon}/k_{scon}) \times (k_{\tau s}/k_{\tau r}) \times k_{\rho s}} \quad (8)$$

where k_{rcon} is the hydraulic conductivity of roots, k_{scon} is the hydraulic conductivity of sapwood, $k_{\tau s}$ is the longevity of sapwood and $k_{\tau r}$ is the root longevity. Following substitution of Eq. (4) into Eq. (7) and some rearrangement, leaf mass can be written as a function of root mass:

$$M_l = f_{LF} \times M_r \quad (9)$$

where,

$$f_{LF} = k_{sar} \times f_{KF} \quad (10)$$

Parameter values used in Eqs. (1) to (9), i.e., k_{lsmax}, k_{lsmin}, k_{sar}, k_{sla}, $k_{\rho s}$, k_{rcon}, k_{scon}, $k_{\tau s}$ and $k_{\tau r}$, are based on literature review (Tables 3 and 4). The allometric relationships between the plant components and the hydraulic architecture of the plant are both based on the pipe model theory, hence, the same parameter values for the hydraulic conductivities of the plant components were used in their calculations.

In this version of ORCHIDEE, forests are modelled to have k_{ncirc} circumference classes with d_{ind} identical trees in each one. Hence, the allocatable biomass (M_{totinc}) needs to be distributed across I diameter classes:

$$M_{totinc} = \sum(I)[d_{ind(I)} \times M_{inc(I)}] \quad (11)$$

where $M_{inc(I)}$ is the biomass that can be allocated to diameter class I. Mass conservation thus requires:

$$M_{inc(I)} = M_{linc(I)} + M_{rinc(I)} + M_{sinc(I)} \quad (12)$$

where $M_{linc(I)}$, $M_{rinc(I)}$ and, $M_{sinc(I)}$ are the increase in leaf, root and wood biomass for a tree in diameter class I, respectively. Eqs. (4) and (8) can be rewritten as

$$\left(M_{l(I)} + M_{linc(I)}\right) / \left(M_{s(I)} + M_{sinc(I)}\right) = f_{KF} / \left(d_{h(I)} + d_{hinc(I)}\right) \quad (13)$$

$$\left(M_{l(I)} + M_{linc(I)}\right) = \left(M_{r(I)} + M_{rinc(I)}\right) \times f_{LF} \quad (14)$$

An allometric relationship is used to describe the relationship between tree height and basal area:

$$d_{h(I)} = k_{\alpha 1} \times \left(4/\pi \times d_{ba(I)}\right)^{(k_{\beta 1}/2)} \quad (15)$$

The change in height is then calculated as

$$d_{hinc(I)} = \left[k_{\alpha 1} \times \left(4/\pi \times \left(d_{ba(I)} + d_{bainc(I)}\right)\right)^{(k_{\beta 1}/2)}\right] - d_{h(I)} \quad (16)$$

where $d_{ba(I)}$ and $d_{bainc(I)}$ are the basal area and its increment, respectively. The distribution of C across the I diameter classes depends on the basal area of the model tree within each diameter class. Trees with a large basal area are assigned more carbon for wood allocation than trees with a small basal area, according to the method of Deleuze et al. (2004).

$$d_{bainc(I)} = f_\gamma \times \left(d_{circ(I)} - k_m \cdot g_\sigma + \sqrt{\left(k_m \times g_\sigma + d_{circ(I)}\right)^2 - \left(4 \times g_\sigma \times d_{circ(I)}\right)}\right)/2 \quad (17)$$

where k_m is a parameter, f_γ and g_σ are calculated from parameters and $d_{circ(I)}$ is the circumference of the model tree in diameter class I. g_σ is a function of the diameter distribution of the stand at a given time step.

Equations (10) to (16) need to be simultaneously solved. An iterative scheme was avoided by linearising Eq. (15), which was found to be an acceptable numerical approximation as allocation is calculated at a daily time step, and hence the changes in height are small and the relationship is locally linear:

$$d_{\mathrm{hinc}(l)} = d_{\mathrm{bainc}(l)} / f_{\mathrm{s}} \tag{18}$$

where f_{s} is the slope of the locally linearised Eq. (15) and is calculated as:

$$f_{\mathrm{s}} = k_{\mathrm{step}} / \left(k_{\alpha 1} \times (4/\pi \cdot (d_{\mathrm{ba}} + k_{\mathrm{step}}))^{(k_{\beta 1}/2)} - k_{\alpha 1} \times (4/\pi \times d_{\mathrm{ba}})^{(k_{\beta 1}/2)} \right) \tag{19}$$

Equations (10)–(14) and (16)–(18) are then solved for f_γ. f_γ distributes photosynthates across the different diameter classes and as such controls the intra-species competition within a stand. f_γ thus depends on the total allocatable carbon and needs to be optimised at every time step. Once f_γ has been calculated, $M_{\mathrm{linc}(l)}$, $M_{\mathrm{rinc}(l)}$ and $M_{\mathrm{sinc}(l)}$ can be calculated.

The different biomass pools have different turnover times, and therefore at the end of the daily time step, the actual biomass components may no longer respect the allometric relationships. Consequently, at the start of the time step carbon is first allocated to restore the allometric relationships before the remaining carbon is allocated in the above manner.

3.2 Hydraulic architecture

The representation of the impact of soil moisture stress on water, carbon and energy fluxes has been identified as one of the major uncertainties in land surface models (De Kauwe et al., 2013). Neither the empirical functions nor the soil moisture stress functions, which are commonly used in land surface models, fully capture stomatal closure and limitation of C uptake during drought stress (Bonan et al., 2014; Verhoef and Egea, 2014). Therefore, we replaced the soil moisture stress function which limits

C assimilation through a constrain on k_{Vcmax} in the ORCHIDEE-trunk, by a constrain based on the amount of water plants can transport from the soil to their leaves.

The model calculates plant water supply according to the implementation of hydraulic architecture by Hickler et al. (2006). Plant water supply is the amount of water the plant can transport from the soil to its stomata, accounting for the resistances to water transport in the roots, sapwood and leaves. If transpiration rate exceeds plant water supply, the stomatal conductance is reduced until equilibrium is reached.

The water flow from the soil to the leaves is driven by a gradient of decreasing water potential. Using Darcy's law (Slatyer, 1967; Whitehead, 1998), the supply of water for transpiration through stomata can be described as:

$$F_{\mathrm{Trs}} = p_{\mathrm{delta}} / \left(R_{\mathrm{r}} + R_{\mathrm{sap}} + R_{\mathrm{l}} \right) \tag{20}$$

where p_δ is the pressure difference between the soil and the leaves; and R_{r}, R_{sap} and R_{l} are the hydraulic resistances of fine roots, sapwood and leaves, respectively. p_{delta} is calculated following Whitehead (1998):

$$p_{\mathrm{delta}} = p_{\psi \mathrm{sr}} - k_{\psi \mathrm{l}} - (d_{\mathrm{h}} \times k_{\rho \mathrm{w}} \times k_{\mathrm{g}}) \tag{21}$$

where $k_{\psi \mathrm{l}}$ is a PFT-specific minimal leaf water potential, which means that plants are assumed to maximise water uptake by lowering their $k_{\psi \mathrm{l}}$ to the minimum, if transpiration exceeds F_{Trs} (Tyree and Sperry, 1989). The product of d_{h}, $k_{\rho \mathrm{w}}$ and k_{g} accounts for the loss in water potential by lifting a mass of water from the soil to the place of transpiration at height d_{h}, $k_{\rho \mathrm{w}}$ is the density of water, and k_{g} is the gravitational constant. The soil water potential in the rooting zone ($p_{\psi \mathrm{sr}}$) was calculated by adding a modulator (m_ψ) to the bulk soil water potential, which was calculated as the sum of the soil water potential in each soil layer weighted by the relative share of roots (d_{rd}) in the individual soil layer:

$$p_{\psi \mathrm{sr}} = \sum (l)[p_{\psi \mathrm{s}} \times d_{\mathrm{rd}}] + m_\psi \tag{22}$$

The soil water potential for each layer $p_{\psi sl}$ is calculated from soil water content according to Van Genuchten (1980).

$$p_{\psi s(l)} = \frac{1}{k_{av}} \left(\left(\frac{M_{swc} - k_{swcr}}{k_{swcs} - k_{swcr}} \right)^{-1/k_{mv}} - 1 \right)^{1/k_{nv}} \quad (23)$$

where M_{swc} is the volumetric soil water content, k_{swcr} and k_{swcs} are respectively the residual and saturated soil water content and k_{av}, k_{mv} and k_{nv} are parameters.

Root resistance is related to the root mass and thus can be expressed as Weatherly (1982):

$$R_r = \frac{1}{(k_{rcon} \times M_r)} \quad (24)$$

where k_{rcon} is the fine root hydraulic conductivity per unit biomass. Sapwood resistance is calculated according to Magnani et al. (2000):

$$R_{sap} = \frac{d_h}{(d_s \times k_{scon})} \quad (25)$$

where k_{scon} is the sapwood specific conductivity, which is decreased when cavitation occurs. The loss of conductance as a result of cavitation is a function of $p_{\psi sr}$ and was implemented by using an s-shaped vulnerability curve:

$$k_{scon} = k_{scon} \times e^{(-p_{\psi rs}/k_{\psi 50})^{k_c}} \quad (26)$$

where $k_{\psi 50}$ is the $p_{\psi sr}$ that causes 50 % loss of conductance; and k_c is a shape parameter.

R_l is related to the specific leaf conductivity per unit leaf area (k_l) and the leaf area index:

$$R_l = \frac{1}{(k_{lcon} \times d_{LAI})} \quad (27)$$

The response of water viscosity to low temperatures increases the resistance (Cochard et al., 2000). The relationship is described as:

$$R_{temp} = \frac{R}{(k_{\alpha 1v} + k_{\alpha 2v} \times T)} \quad (28)$$

where $k_{\alpha 1v}$ and $k_{\alpha 2v}$ are empirical parameters (Cochard et al., 2000), R_{temp} is the temperature adjusted R_l, R_{sap} or R_r, T is air temperature for R_l and R_{sap} and T is soil temperature for R_r.

If, for any time step, the transpiration calculated by the energy budget exceeds the amount of water the plant can transport from the soil to its stomata, transpiration is limited to the plant water supply. As the transpiration is now reduced, the initial calculations of the energy budget and photosynthesis, solely based on atmospheric information, are no longer valid. As a result the energy budget and photosynthesis must be recalculated for the time step in question. For this recalculation, stomatal conductance at the canopy level is calculated such that transpiration equals the amount of water the plant can transport. Owing to the feedback between stomatal conductance, leaf surface temperature and transpiration this calculation may require up to 10 iterations to converge. Canopy level stomatal conductance is then decomposed to obtain the stomatal conductance at each canopy layer assuming that each layer is equally restricted by drought stress. Finally, the restricted stomatal conductance is used to calculate CO_2 assimilation rate according to the photosynthesis model by Farquhar, von Caemmerer and Berry (see Sect. 3.6).

3.3 Canopy structure

Stand structure controls the amount of light that penetrates to a given depth in the canopy. For example, the amount of light reaching the forest floor will be higher for a stand with few mature trees compared to many young trees even if both stands have the same leaf area index. Where a big leaf approach assumes a homogeneous block shaped canopy (as in the trunk version of ORCHIDEE) and can therefore rely

on the law of Beer-Lambert, a geometric approach is required to calculate light penetration through structured canopies. Light penetration needs to be simulated to calculate albedo (see Sect. 3.4), photosynthesis (see Sect. 3.6), partitioning of energy fluxes (see Sect. 3.5) and the amount of light reaching the forest floor (see for example Sect. 3.1). The gap fraction, which is the basic information in calculating light penetration at different depths in the canopy, is calculated following the approach presented by Haverd et al. (2012) and formalized in their semi-analytical model. Rather than a spatially explicit approach, Haverd et al. (2012) follow a statistical approach which reduces the memory requirements for the simulations and limits the space requirements for storing the model output files.

The model of Haverd et al. (2012) represents the canopy by a statistical height distribution with varying crown sizes and stem diameters for each height class. The crown canopies are treated as spheroids containing homogeneously distributed single scatterers. Although this f_{Pgap} model can explicitly include trunks, we made the decision to exclude them, as the spectral parameters for our radiation model (see Sect. 3.4) are extracted from remote sensing data (see Sect. 4.8) without distinguishing between leafy and woody masses. This gives the gap probability for trees as a function of height (z) and solar zenith angle (θ_{z}):

$$f_{\mathrm{Pgap}}^{\mathrm{trees}}(\theta_{\mathrm{z}}, z) = e^{(-d_{\lambda} \times \overline{d_{\mathrm{c}}}(\theta_{\mathrm{z}}, z) \times (1 - \overline{f_{\mathrm{Pwc}}}(\theta_{\mathrm{z}}, z)))} \tag{29}$$

where d_{λ} is the inverse of the tree density, d_{c} is the projected crown area (for an opaque canopy), and f_{Pwc} is the mean crown porosity. The overbar depicts the mean over the tree distribution as a function of tree height or, in our case, the mean over the l circumference classes. Following minor adaptations, the implementation of Haverd and Lovell (Haverd et al., 2012) was incorporated in ORCHIDEE-CAN. As there also exist crops, grasses, and bare soil in the model, f_{Pgap} was adjusted for these situations as well. For grasses and crops, the same formulation is used:

$$f_{\mathrm{Pgap}}^{\mathrm{gc}}(\theta_{\mathrm{z}}, z) = e^{(-0.5 \times d_{\mathrm{LAIabove}} \times m_{\mathrm{LAIcorr}} / \cos(\theta_{\mathrm{z}}))} \tag{30}$$

where d_{LAIabove} is the total amount of LAI above height z, and m_{LAIcorr} is a correction factor to account for the fact that grasses and crops are treated as homogeneous blocks of vegetation with no internal structure and is often referred to as a clumping factor. Here it is treated as a tunable parameter and therefore the term correction factor was used. For bare soil, there is no vegetation to intercept radiation, and therefore $f_{\mathrm{Pgap}}^{\mathrm{bs}}(\theta_{\mathrm{z}}, z)$ is always unity.

3.4 Multi-layer two-way albedo for tall canopies

Species-specific radiation absorbance, reflectance and transmittance by the forest canopy were calculated from a radiation transfer model (Pinty et al., 2006) which was parametrized by satellite-derived species-specific scattering values (see Sect. 4.8). Given the complexity of radiation transfer, it remains challenging to accurately simulate radiation transfer through structurally and optically complex vegetation canopies without using explicit 3-D models. The applied 1-D model belongs to the family of two-stream models (Meador and Weaver, 1980) and thus calculates transmittance, absorbance and reflectance of both the incoming and outgoing radiation. The calculation of the reflectance at the top of the canopy due to a collimated source (i.e., the sun) is divided in three components:

1. scattering of radiation between the vegetated elements with a black background

$$f_{\mathrm{Coll,\,veg}}^{f_{\mathrm{R}}} = f(\theta_{\mathrm{mu}}, f_{\mathrm{rl}}, f_{\mathrm{tl}}, g_{\mathrm{G}}, d_{\mathrm{LAIeff}}) \tag{31}$$

2. scattering of radiation by the background with a black canopy

$$f_{\mathrm{UnColl,\,bgd}}^{f_{\mathrm{R}}} = f_{\mathrm{Rbgd}} \times e^{(-d_{\mathrm{LAIeff}}/(2 \times \theta_{\mathrm{mu}}))} \times f_{\mathrm{UnColl,\,veg}}^{\mathrm{T}} \tag{32}$$

3. multiple scattering of radiation between the canopy and the background

$$f_{\mathrm{Coll,\,bgd}}^{f_{\mathrm{R}}} = f_{\mathrm{Rbgd}} \times \left[f_{\mathrm{Coll,\,bgd,1}}^{f_{\mathrm{R}}} + f_{\mathrm{Coll,\,bgd},n}^{f_{\mathrm{R}}} \right] \tag{33}$$

Term (1) is widely used in cloud reflectance calculations, and depends on the cosine of the solar zenith angle (θ_{mu}), the reflectance and transmittance of the single leaves (f_{rl} and f_{tl}, respectively), the leaf orientation function (g_G), and the effective LAI (d_{LAIeff}). The exact definition of this term is given in Eq. (B2) in Pinty et al. (2006). In term (2), f_{Rbgd} is the reflectance of the ground beneath the canopy and $f^{T}_{UnColl,\,veg}$ is the transmitted fraction of light to the ground which has not collided with any canopy elements. In term (3), $f^{f_R}_{Coll,\,bgd,1}$ is the fraction of light which has struck vegetation and collided with the background a single time, while $f^{f_R}_{Coll,\,bgd,n}$ is the fraction which has collided multiple times (n) with the background. The sum of the three components results in the canopy albedo (Pinty et al., 2006). Similar equations can be derived for light originating from diffuse sources (e.g., clouds and other atmospheric scattering). Implementations of the calculations of the canopy fluxes for a single level are available from the JRC, and these implementations were used as the basis of the routines put into ORCHIDEE-CAN for both the single- and multi-level cases (McGrath et al., 2014). This implementation relies on the use of the effective LAI, which is the LAI that needs to be used in a 1-D process representation to obtain the same reflectance, absorbance and transmittance as would be obtained by a 3-D-canopy representation (Pinty, 2004). In this study, the effective LAI was calculated by first computing the canopy gap probability, i.e. the probability that light is transmitted to a specified height in the canopy at a given solar angle. The gap probability is then converted into the effective LAI by passing it as an input to the inverted Beer-Lambert's law (with an assumed extinction coefficient of 0.5).

$$d_{LAIeff} = -2.0 \times \cos(\theta_z) \times \log(f_{Pgap}) \tag{34}$$

where f_{Pgap} can be f^{trees}_{Pgap}, f^{gc}_{Pgap}, f^{bs}_{Pgap}. Following the introduction of multi-layer photosynthesis and energy budget submodels, the approach proposed by Pinty (2004) had to be adjusted such that it could be applied for every level for which absorbance needs to be known to calculate photosynthesis (see Sect. 3.6) and reflectance needs to be known to calculate the net shortwave radiation (see Sect. 3.5). The multi-layer approach basically applies the 1-D-two stream canopy radiation transfer model by Pinty et al. (2006) to each canopy level where the light transmitted by the overlaying level becomes the input for the lower level.

As the multi-level approach is built around the solution of the one-level scheme for each canopy level, no new equations are introduced. The method can be summarized by the following algorithm for which the details are given in (McGrath et al., 2014). First, three fluxes are calculated for each level independently: the fraction of light transmitted through the layer without striking vegetation, the fraction of light reflected after striking vegetation, and the fraction of light transmitted through the layer after striking vegetation. These three fluxes represent the only possible fate of light (any light not taking one of these paths must be absorbed for energy conservation). Next, an iterative approach is invoked which follows the path of a single photon entering the top level. Based on the solutions for each single level, probabilities can be calculated that the photon is transmitted to a lower level or reflected to a higher level. Any fraction which is reflected upwards from the top level is added to the total canopy albedo and not considered further. The fraction which is transmitted through the top level enters the next highest level, and again the single level solutions determine where this light goes. Any fraction reflected upwards is considered in the next iteration as part of the light entering the upper level. The steps continue until the bottom canopy level is reached. Here, any fraction which is transmitted into the soil is removed from consideration and added to the total transmittance through the canopy. The algorithm then proceeds to the above canopy level. Now the "transmitted" fluxes are moving in the upwards direction towards to the sky, while "reflected fluxes" are moving towards the ground. The code continues towards the top level, taking as input from below both the flux reflected by downwelling light from the level below the current level and the flux transmitted from the lower level by upwelling light. After each iteration (moving from the top of the canopy to the bottom and back to the top), the total amount of light considered "active" has been reduced by light escaping to the sky or being absorbed by the canopy or ground. Eventually, this

"active" light falls below a pre-defined threshold and the calculation is considered as converged.

Due to the iterative procedure, energy is not strictly conserved, although we have attempted to choose a threshold which minimizes this loss. The multilevel albedo calculation is currently the most expensive part of the model, due to the iterations and the fact that it must be performed over all canopy levels (currently set to 10), grid points, and PFTs at every physical time-step. Levels with no LAI are no less expensive to compute, either, although we have arranged our canopy levels to make sure no levels are empty in most cases.

3.5 Multi-layer energy budget

The present generation of land surface models have difficulties in reproducing consistently the energy balances that are observed in field studies (Pitman et al., 2009; Jiménez et al., 2011; de Noblet-Ducoudré et al., 2012). The ORCHIDEE-CAN branch implemented an energy budget scheme that represents more than one canopy layer to simulate the effects of scalar gradients within the canopy for determining more accurately the net sensible and latent heat fluxes that are passed to the atmosphere. As outlined in Polcher et al. (1998), the use of an implicit solution for coupling between the atmospheric model and the surface layer model is the only way to keep profiles of temperature and humidity synchronised across the two models when the coupled-model is run over large time steps (e.g., of 30 min). The difference between explicit and implicit schemes is that an explicit scheme will calculate each value of the variable (e.g., temperature and humidity) at the current time step entirely in terms of values from the previous time step. An implicit scheme requires the solution of equations written only in terms of those at the current time step.

The modelling approach formalises three constraints that ensure energy conservation. The three equations that describe the main interactions are:

1. the energy balance at each layer is the sum of incoming and outgoing fluxes of latent and sensible heat and of shortwave and longwave radiation:

$$k_{\mathrm{lhc},i} k_{\rho_\mathrm{v},i} \frac{\delta T_{\mathrm{L},i}}{\delta t} = \left(k_{\mathrm{shc}} k_{\rho_\mathrm{a}} \frac{(T_{\mathrm{L},i} - T_{\mathrm{a},i})}{R_{\mathrm{a},i}} + k_{\lambda,\mathrm{LE}} \rho_\mathrm{a} \frac{q_{\mathrm{L},i} - q_{\mathrm{a},i}}{R_{\mathrm{s},i}} + F_{\mathrm{SW},i} + F_{\mathrm{LW},i} \right) \left(\frac{1}{\Delta d_{\mathrm{hl},i}} \right) \quad (35)$$

   where $F_{\mathrm{LW},i}$ is the sum total of long wave radiation, that is, the net LW radiation absorbed into layer i and $F_{\mathrm{SW},i}$ is the net absorbed short wave radiation as calculated by the albedo scheme in Sect. 3.4. k_{shc} is the specific heat capacity of air. The source sensible heat flux from the leaf at level i is the difference between the leaf temperature ($T_{\mathrm{L},i}$) and the atmospheric temperature at the same level ($T_{\mathrm{a},i}$), divided by $R_{\mathrm{a},i}$, which is the leaf resistance to sensible heat flux (a combination of stomatal and boundary layer resistance). Similarly, the source latent heat flux from the leaf at level i is the difference between the saturated humidity in the leaf ($q_{\mathrm{L},i}$) and that in the atmosphere at level i ($q_{\mathrm{a},i}$), divided by $R_{\mathrm{s},i}$ which is the leaf resistance to latent heat flux. $R_{\mathrm{a},i}$ is calculated based upon the leaf boundary layer resistance, and is described in the present model according to Baldocchi (1988). $R_{\mathrm{s},i}$ is the stomatal resistance of the leaf that may be calculated using the model of Ball et al. (1987).

2. Transport of sensible heat flux between the vegetation ("the leaf") and the surrounding atmosphere at each level, and between adjacent atmospheric levels above and below is provided by the following expression:

$$\frac{\delta T_{\mathrm{a},i}}{\delta t} \Delta d_{\mathrm{V},i} = k_{\mathrm{k},i} \frac{\delta^2 T_{\mathrm{a},i}}{\delta z^2} \Delta d_{\mathrm{A},i} + \left(\frac{T_{\mathrm{L},i} - T_{\mathrm{a},i}}{R_{\mathrm{a},i}} \right) \left(\frac{1}{\Delta d_{\mathrm{hl},i}} \right) \Delta d_{\mathrm{V},i} \quad (36)$$

   where z denotes the height above the soil suface. We have re-written the scalar conservation equation, as applied to canopies, in terms of the sensible heat flux, temperature and source sensible heat from the vegetation at each layer.

3. The transport of latent heat flux between the vegetation and surrounding atmosphere at each level, and between adjacent atmospheric levels above and below is described in a form that is analogous to Eq. (36), above:

$$\frac{\delta q_{\mathrm{a},i}}{\delta t}\Delta d_{\mathrm{V},i} = k_{\mathrm{k},i}\frac{\delta^2 q_{\mathrm{a},i}}{\delta z^2}\Delta d_{\mathrm{A}_i} + \left(\frac{q_{\mathrm{L},i} - q_{\mathrm{a},i}}{R_{\mathrm{s},i}}\right)\left(\frac{1}{\Delta d_{\mathrm{hl},i}}\right)\Delta d_{V_i} \quad (37)$$

In addition to these three basic equations various terms had to be parameterised. The 1-D second-order closure model of Massman and Weil (1999) was used to simulate the vertical transport coefficients $k_{\mathrm{k},i}$ within the canopy while accounting for the vertical and horizontal distribution of LAI (see Sect. 3.3). This set of equations were then written in an implicit form and solved by induction. More details on the implicit multi-layer energy budget and a complete mathematical documentation are given in Ryder et al. (2014).

To complete the energy budget calculations, the multi-layer 1-D canopy radiation transfer model (see Sect. 3.4) was used to calculate the net shortwave radiation at each canopy layer. Further, the canopy radiation scheme makes use of the Longwave Radiation Transfer Matrix (LRTM) (Gu, 1988; Gu et al., 1999). This approach separates the calculation of the radiation distribution completely from the implicit expression. Instead, a single source term for the long wave radiation is added at each level. This means that the distribution of LW radiation is now explicit (i.e., makes use of information only from the "previous" and not the "current" time step) but the changes within the timestep were small enough to not affect the overall stability of the model). However, an advantage of the approach is that it accounts for a higher order of reflections from adjacent levels than the single order assumed in the process above.

3.6 Analytical solution for photosynthesis

The photosynthesis model by Farquhar, von Caemmerer and Berry (Farquhar et al., 1980) predicts net photosynthesis of C3 plants as the minimum of the Rubisco-limited

rate of CO_2 assimilation and the electron transport-limited rate of CO_2 assimilation (Farquhar et al., 1980). The ORCHIDEE-CAN branch calculates net photosynthesis following an analytical algorithm as described by Yin and Struik (2009). In addition, the C4 photosynthesis is calculated by an equivalent version of the Farquhar, von Caemmerer and Berry model that was extended to account for noncyclic electron transport (Yin and Struik, 2009). A detailed derivation of the analytical solution of the Farquhar, von Caemmerer and Berry model is given in Yin and Struik (2009).

Owing to the canopy structure simulated in this model version and the layering of the canopy, the amount of absorbed light now varies with canopy depth. This new approach replaces the old scheme which uses multiple levels based on the leaf area index, not the physical height within the canopy. Photosynthesis is now calculated at each vertically resolved canopy level independently, using the total amount of absorbed light calculated by the radiation transfer scheme, which means that radiation transfer inside the canopy and photosynthesis are now fully consistent. In the new photosynthesis scheme, photosynthesis thus indirectly depends on canopy structure.

3.7 Mortality

A variety of changes have been made to processes involving vegetation death. A whole PFT is now killed if, at the end of the day, there is no carbon available in leaf, carbohydrate reserve, or labile pools. In this situation, it will be impossible for the plant to assimilate new carbon from the atmosphere as it will not be able to grow new leaves and thus initiate plant recovery. In addition, a forest can die if the density falls below a certain prescribed value. In the next time step a new young forest will be prescribed. Different age classes are distinguished to better account for the structural diversity and its possible effects on the element, energy and water fluxes. A clear hierarchy was established for the mortality processes when it comes time to actually kill the trees (i.e., move their biomass to the litter or harvest pools). All of the processes determine first how much biomass they would remove in the absence of all the other processes. Afterwards, the killing is arranged in the most realistic way possible. A clear-cut event

has the highest priority, followed by human thinning and finally natural mortality including self-thinning. If, for example, a forest is scheduled to be clear-cut, the entire forest biomass is subjected to the rules of the clear-cut and no other mortality occurs in that time-step.

If a forest is thinned, it is assumed that the weakest trees will be thinned, and therefore human thinning reduces or even eliminates the natural mortality for that time-step. Natural mortality still happens on a daily time-step, while human-induced mortality happens only at the end of the year. Self-thinning, as described below, takes priority over environmental mortality. Environmental mortality is calculated as a fraction of the total site biomass; if self-thinning is greater than or equal to this percentage, no environmental mortality occurs in this time-step. Otherwise trees are selected so that the total amount of biomass killed due to self-thinning and environmental mortality is equal to the total amount predicted by multiplying the stand biomass by the mortality percentage.

The use of circumference classes adds a good deal of realism and flexibility to the ORCHIDEE-CAN simulations, but it also raises additional questions. For example, which trees should be targeted by which mortality? Given that self-thinning reflects the outcome of continuous resource competition, the largest trees are expected to be most successful when competing for resources, and therefore we mainly kill the smallest trees to reduce the stand density. Conversely, larger trees are more likely to die because of environmental stress factors, being more prone to cavitation, wind damage, lightening, and, heart rot. Therefore, we select more older trees to die from environmental mortality. While doing this also trees in the other diameter classes were killed based on the following recursive definition (cf. Bellassen et al., 2010):

$$f_{\text{death}}^{\text{icir}} = \frac{f_{\text{death}}^{\text{icir}-1} \times k_{\text{ddf}}^{1-(k_{\text{ncirc}}-1)}}{m_{\text{Ndeath}}} \tag{38}$$

where k_{ddf} is the death distribution factor, which is the factor by which the smallest and largest circumference classes differ (e.g., $k_{\text{ddf}} = 10$ means that the largest circumference class will lose ten times as much biomass as the smallest as a result of the mortality), m_{Ndeath} is a normalization factor so that sum of $f_{\text{death}}^{\text{icir}}$ is unity, and f_{death}^{1} is set equal to unity before normalization. As the stands are very close to even-aged, we set the factor k_{ddf} to be equal to 1. This means the same number of trees is killed in each circumference class If, for some reason, there is not enough biomass in a given class to satisfy this distribution, the extra biomass is taken from the next smallest class (in the case the smallest class does not have enough, it is taken from the largest class).

Related to mortality is the question of the circumference class distribution. As mentioned above, trees in different circumference classes are preferentially killed by different processes. If the simulation is long enough (or if the morality is aggressive enough), eventually the number of trees in some circumference classes may become zero. This would reduce the numerical resolution of the allocation scheme. When only one circumference remains populated, the scheme effectively loses its meaning as all the newly produced biomass is now be allocated to the only remaining circumference class. In order to maintain the same level of detail through the simulation, the distribution of all the circumference classes is recalculated at the end of each day. A normalized target distribution is specified as an input parameter (an exponential distribution is currently used), and this distribution is scaled to produce a target distribution for the current number of individuals. All of the current individuals are placed in these new classes until the target distribution is satisfied. The target distribution now contains, however, trees of multiple sizes, so we need to average them to find the new "model" tree for each class. By changing the size of the model tree in each class, we are able to preserve the total biomass of the stand as well as the total number of individuals.

4 Description of the parametrization

The ORCHIDEE-CAN branch was specifically developed to quantify the climate effects of forest management over Europe. Although the developments are sufficiently general to be applied outside of Europe, the model was initially parametrized for the

boreal, temperate and Mediterranean climate zones and validation focused on Europe. Parametrization of the tropical zone is subject of a follow-up study.

4.1 Introducing twelve new PFTs

Similar to the ORCHIDEE trunk, the ORCHIDEE-CAN branch distinguishes 13 meta-
5 classes (MTC) for vegetation. Outside Europe the original MTC classification of ORCHIDEE was kept, while inside Europe 12 new parameter sets representing the main European tree species were added. The default vegetation distribution map in ORCHIDEE, i.e., Olson et al. (1983), was replaced by an up-to-date global MTC map which has been produced using the ESA CCI ECV Land Cover map (http://www.
10 esa-landcover-cci.org/)(Poulter et al., 2014).The mapping from land cover to MTC basically followed Poulter et al. (2011), although Table 5 (the "cross-walking" table) has been updated following discussions with the LC_CCI team at Universite Catholique de Louvain. For the European domain, the global MTC distribution was overlaid by a tree species distribution map (Brus et al., 2012).

15 This study focusses on tree species with a coverage of more than 2 % in Europe, yielding seven species groups covering in total 78.8 % of the European forest area: *Betula sp.*, *Fagus sylvatica*, *Pinus sylvestris*, *Picea sp.*, *Pinus pinaster*, *Quercus ilex* and a group combining *Quercus robur* and *Quercus petraea*. For *Pinus sylvestris*, *Picea sp.* and *Betula sp.* An additional distinction between boreal and temperate forest was
20 made for the species map and parametrization: trees located in Norway, Sweden and Finland were considered boreal, while trees growing at lower latitudes were categorized as temperate. Given the potential role of tree species of the Salicacea genus in short rotation coppice management, a separate PFT was parametrized for *Populus sp.* Furthermore, to improve the parametrization of the MTC of boreal needleaved
25 deciduous forest, observations from *Larix sp.* were included when possible.

For these 12 forest species, 12 new PFTs were created with each PFT belonging to a single MTC (see Tables 4, 5, 6) Almost 79 % of the European forest was parametrized at the species level. The remaining 21 % was reclassified in four residual groups, i.e.,

a temperate and boreal needleleaf evergreen and a temperate and boreal broadleaved residual group. For use outside Europe, the original MTC classification of ORCHIDEE was kept. The parameters of the residual groups and MTCs are the mean of the parameters of the species-level PFTs that are in the MTC, with the exception of albedo
5 parameters that could be extracted from remote sensing products.

Finally, separate PFTs were introduced for boreal grasses and croplands, which allowed for a boreal parametrization of phenology, senescence and growth. This approach, which distinguishes a total of 28 PFTs, allows a higher taxonomic resolution over Europe, better defines forest types compared to the more general MTC approach
10 and facilitates the use of observations to derive parameters.

4.2 Sources of parameter values

Species parameters were extracted from a wide range of sources including original observations (i.e. POPFULL), large databases (national forest inventories, TRY), primary research reports and remote sensing products (JRC-TIP Pinty et al., 2011a, b).
15 The mean values and standard deviations were calculated without weighting. For most parameters, the mean values were used as the parameter value in ORCHIDEE without further processing. Using the mean parameter estimates at the species level avoids hidden model-tuning and largely reduces the likelihood that simulation results are biased by hidden calibration owing to a poor taxonomic definition of PFTs (Scheiter et al.,
20 2013). The phenology-related parameters of the deciduous MTCs were optimised by MacBean et al. (2014), using MODIS-derived NDVI data normalised to model fAPAR over the 2000–2008 time period.

4.3 Selection of parameters for optimization

The vegetation structure simulated by the ORCHIDEE-CAN branch is sensitive to the
25 value of k_{ls} which describes the ratio between the leaf and sapwood area of an individual tree. The available observations show a wide range within and across species.

Dependencies of k_{ls} on tree height (McDowell et al., 2002; Novick et al., 2009), tree diameter following stand thinning (Simonin et al., 2006) and CO_2 (Pataki et al., 2006) have been reported. Most observations come from experiments where time was substituted by space which hampers teasing apart the sources of variability. Given the variation and uncertainty in the observations and the model sensitivity to this parameter, we tuned its value within the observed range to jointly match European-wide observations of GPP, evapotranspiration and effective leaf area index.

Both the trunk and ORCHIDEE-CAN branch reduce the definition of net primary production to biomass production; hence, carbon leaching from the roots, volatile organic emissions from the leaves, dissolved and particulate carbon losses through water fluxes and carbon subsidies to mycorryhzae are not accounted for in the model. These fluxes are (incorrectly) accounted for in the modelled autotrophic respiration. Modelled autotrophic respiration should therefore be considered an effective rather than a true value. For this reason, the basal rate of autotrophic respiration was optimized against site observations of biomass production efficiency (i.e., the ratio between annual biomass production and annual photosynthesis), using an optimization scheme that minimizes the mismatch between the model and the observations in a rigorous statistical framework (see for example Tarantola, 2005).

4.4 Allocation

In addition to k_{ls} the leaf to sapwood area, the allocation scheme required several new parameter values that were estimated from fitting regression models to the national forest inventory data of Spain, France, Germany and Sweden or through literature search (Table 4).

Strictly speaking, the basal rate of autotrophic respiration is not an allocation parameter but here it was optimized against 126 site observations of the biomass production efficiency (k_{cmaint}, Table 3) calculated as the ratio between annual biomass production and annual photosynthesis (Vicca et al., 2012; Campioli et al., 2014). Where the model now simulates an acceptable GPP, it will also simulate an acceptable biomass

production which justifies the inclusion of this respiration parameter in the section on allocation. Following this approach it remains untested how well the simulated effective autotrophic respiration represents the (rarely) observed autotrophic respiration. Note that in the cases of both the trunk and the ORCHIDEE-CAN branch of ORCHIDEE, a match between effective and observed autotrophic respiration should not be interpreted as evidence of desired model behaviour because several components of net primary production are not modelled yet (see Sect. 4.3).

4.5 Hydraulic architecture

Initial choices of parameters for this scheme were based on the values and parameter sources listed by Hickler et al. (2006). All data sources were revisited and the search was extended to obtain values at the PFT rather than MTC level (Table 4). Given that plant hydraulogy is rather well studied, observed parameters were available for most of the species. Our implementation of hydraulic architecture required the introduction of a tuning parameter to account for processes that are currently absent in, e.g. plant water storage and soil-root resistance. A more process-based description of these processes (i.e., Sperry et al., 1998; Steppe et al., 2005) is being tested and should allow removal of this parameter.

4.6 Canopy structure

The relationship between diameter and projected crown surface area follows the model proposed by Pretzsch (2009):

$$d_{csa} = k_{ap} \times d_{dbh}^{k_{bp}} \tag{39}$$

with parameters estimated using the dataset presented in Pretzsch and Dieler (2012). This dataset contains diameter and projected crown surface areas observations for over 30 000 individual trees in Europe covering almost 30 species. Species-specific

observations were used to fit the species-specific parameter values (Table 4). Parameter values for MTCs were derived by grouping the species into MTCs and fitting the parameters. No observations were available for the boreal zone and temperate evergreen deciduous species. For the boreal species a subset of the temperate observations (*Pinus sylvestris*, *Picea abies* and *Betula pendula*) was used, i.e., the relationship between d_{csa} and d_{dbh} was fitted to all available data for *Pinus sylvestris.* Next, all observations with a d_{csa} that falls below the predicted d_{csa} were selected as considered to represent a boreal subset. Given the importance of snow pressure on crown structure, selecting observations with sub average d_{csa} is justifiable as a first approximation. Subsequently, the parameters were fitted to this subset of data. For *Quercus ilex* no data were available and parameters were tuned such that the crown diameter was 0.85 m less than the tree height.

4.7 Multi-layer two-way albedo for tall canopies

The radiation transfer scheme makes use of parameters describing leaf and background properties, i.e., leaf single scattering and prefered scattering direction (for both visible (VIS) and near-infrared (NIR) wavelengths) and the so-called background albedo or the albedo of the surface below the dominant tree canopy (VIS and NIR). All parameters were taken from the Joint Research Centre Two-stream Inversion Package (JRC-TIP) (Pinty et al., 2011a, b). This is a software package (Pinty et al., 2007) which inverts a two-stream model (Pinty et al., 2006) to best fit the MODIS broadband visible and near-infrared white sky surface albedo from 2001 to 2010 at 1 km resolution (Pinty et al., 2011a). The inverse procedure implemented in the JRC-TIP is shown to be robust, reliable, and compliant with large-scale processing requirements (Pinty et al., 2011a). Furthermore, this package ensures the physical consistency between sets of observations, the two-stream model parameters, and radiation fluxes.

Only parameter values for which the posterior standard deviation of the probability density functions were significantly smaller than the prior standard deviation were selected from the JRC-TIP since this condition ensures statistically significant values.

Species and MTC specific values were derived from JRC-TIP by performing a multiple regression (Table 6). This methods determines, in an objective way, how the fractions of each MTC or species explain the JRC-TIP parameter. The multiple regression was performed separately for the six parameters: the single scattering of leaves (for both VIS and NIR), the scattering direction of leaves (VIS and NIR) and the background albedo (VIS and NIR). Each JRC-TIP parameter was used as the dependent variable and the independent variables consisted of the fractions of each MTC (Poulter et al., 2014) or species (Brus et al., 2012). These fractions were used to find a linear function that best predicted each JRC-TIP parameter. The corresponding slope of a regression of each MTC or species fraction gives the MTC or species dependent JRC-TIP value. The multiple regression was performed without an intercept. To avoid pollution by the seasonal cycle, the multiple regression was applied only for the pixels of the Northern Hemisphere. Only pixels that were less than 10 % covered by non-vegetative fractions where selected for the analysis and only significant results following an F-test and positive r^2 values were selected.

4.8 Analytical solution for photosynthesis

Three originally MTC-specific photosynthetic parameters (k_{Vcmax}, k_{Jmax} and k_{sla}) were derived at the species level by obtaining weighted site means for each species from the global leaf trait database TRY (Kattge et al., 2011) and additionally from Medlyn et al. (2002). Only k_{Vcmax} and k_{Jmax} standardized to a common formulation and parametrization of the photosynthesis model by (Farquhar et al., 1980) were used. Most k_{Vcmax} and k_{Jmax} values in the TRY database had already been standardized to a reference temperature of 25 °C (Kattge and Knorr, 2007). Subsequently, a species-specific $k_{Jmax,opt}/k_{Vcmax,opt}$ ratio was calculated from the records which included both $k_{Vcmax,opt}$ and $k_{Jmax,opt}$ measurements. From this ratio, which was within a range of 1.91–2.47 for each species, $k_{Jmax,opt}$ was calculated for records which originally only included k_{Vcmax}. Only geo-referenced observations within Europe were used and the distinction between boreal and temperate forest was made similar to the species map.

Depending on the species this resulted in 5 to 183 observations for k_{sla} and 11 to 173 observations for $k_{Vcmax,opt}$ and $k_{Jmax,opt}$. From these observations species-specific means were calculated, weighted for differences in the number of observations per site (Table 5).

4.9 Forest management strategies

Tree mortality is controlled by (see Sect. 3.7): (1) maximum tree diameter, (2) minimum stand density, (3) environmental mortality, (4) self-thinning and, (5) anthropogenic thinning. Maximum tree diameter was extracted from the French, Swedish, German and Spanish forest inventories as the observed 50 % quantile for diameter at breast height. The 50 % quantile rather than the observed maximum was used to account for the fact that large scale land surface models are expected to reproduce large scale patterns rather than local extremes. Minimum stand density was estimated as the expected stand density for the maximum tree diameter for a stand under self-thinning. Although both criteria are related to each other through the observed self-thinning relationship, the minimum number of trees is used to decide when unmanaged forests should be replaced, whereas both the maximum diameter and the minimum number are used for managed sites as criteria to initiate a clear cut.

Self-thinning was parametrized based on the observed relationship between stand density and quadratic mean stand diameter. These observations include mortality due to intra-stand competition which strictly speaking is the process described by the self-thinning relationship as well as the mortality of individuals by insects, lightening, wind, drought, frost and heart rot; these are referred to here as environmental mortality. Because the national forest inventory data rarely distinguish between these causes of mortality we introduced a two step approach. First, self-thinning mortality is calculated. Where self-thinning is less than an assumed constant environmental mortality of $1/k_{t_{resid}}$, self-thinning is complemented by additional mortality to reach the set environmental mortality. Where self-thinning mortality exceeds the set environmental mortality, simulated self-thinning is assumed to include environmental mortality. The fire module

that is available for the trunk but not for the ORCHIDEE-CAN branch simulates stand replacing fires rather than individual-tree based mortality due to lightening. The approach implemented in the ORCHIDEE-CAN branch could therefore be extended with models that simulate stand replacing mortality from fire, insects and storms.

Resource competition between trees in the same stand has been reported to result in the so-called self-thinning relationship that relates the number of individuals within a stand to the stand biomass (Reineke, 1933; Kira et al., 1953; Yoda et al., 1963):

$$(M_s + M_h) \times k_{\rho s} = k_\alpha \times (d_{ind})^{-k_\beta} \quad (40)$$

where k_α and k_β are the constants of the self-thinning relationship. Furthermore, stem volume can be written as a function of tree diameter (d_{dbh}), tree height and stem form factor ($k_{\alpha'}$) to account for the fact that the stem shape is not a perfect cylinder:

$$(M_s + M_h) \cdot k_{\rho s} = k_{\alpha'} \times (d_{dbh})^2 \cdot d_h \quad (41)$$

Following the allometric relationship given in Eq. (14), tree height can be written as a function of tree diameter. Hence, the self-thinning relationship can be re-written to relate stand diameter to stand density:

$$d_{dbh} = k_{\alpha 2} \times (d_{ind})^{-k_{\beta 2}} \quad (42)$$

where, $k_{\beta 2}$ relates to $k_{\beta 1}$ (as in Eq. 14) as follows:

$$k_{\beta 2} = -3/2 \times (2 + k_{\beta 1}) \quad (43)$$

$k_{\alpha 1}$ and $k_{\beta 1}$ were estimated by fitting Eq. (14) to observed diameter and height of individual trees from NFI of Sweden, Germany, France and Spain. $k_{\beta 2}$ was calculated from Eq. (43) and $k_{\alpha 2}$ was estimated by fitting Eq. (42) to observations of the quadratic mean stand diameter and stand density from NFI data.

5 Validation

ORCHIDEE-CAN is designed as the land surface model to be coupled to the atmospheric model LMDz. As such future applications of ORCHIDEE-CAN are expected to be regional to global in the spatial domain and to span several years in the temporal domain. Given its anticipated uses, the ability of the model to reproduce large-scale spatial patterns as well as their inter-annual variability is essential. The first applications of the model, both offline and coupled to the atmosphere, will focus on Europe. The validation, therefore, reports performance indices both over Europe as over eight separate regions within Europe (Bellprat et al., 2012). These eight regions, which partially overlap, are defined after Bellprat et al. (2012). Furthermore, the performance indices are calculated for winter, spring, summer and autumn and thus allow to evaluate the capacity of the model to reproduce observed annual cycles.

In addition to the root mean square error, a land performance index (LPI) based on the principles laid out for the Climate Performance Index (Murphy et al., 2004, their SI) was also calculated. LPI normalizes the root of the squared differences between the simulations and observations by the observed spatial and temporal variance. The LPI was used to estimate the likelihood that the simulated variable belongs to the same population as the observed variable, defined as $\exp(-0.5\mathrm{LPI}^2)$. An LPI equal to 1 indicates that the model correctly reproduces the mean observed value and implies a likelihood of 61 % (Murphy et al., 2004) that the simulations and observations come from the same population. Similarly, an LPI of 2 reduces this likelihood to 13 %. An LPI of less than 0.32 has a likelihood of more than 95 % and therefore indicates a statistically significant result.

While developing ORCHIDEE-CAN, the numerical approaches that added functionality to the code were selected on the basis of their performance at the site-level (see below). Rather than running the same site-level tests for our implementation, we performed a complementary large-scale validation. The strength of our approach lies not in the details, as is the case for site-level validation, but in its width by simultaneously

testing model performance for structural variables such as basal area (de Rigo et al., 2014), canopy structure (Pinty et al., 2011a) and canopy height (Simard et al., 2011), biogeochemical fluxes such as GPP (Jung et al., 2011), biophysical fluxes such as albedo (Schaaf et al., 2002) and fluxes at the interface of biogeochemistry and biophysics such as evapotranspiration (Jung et al., 2011). The selection of variables was limited by the availability of spatially explicit data-derived products for Europe.

For the validation, both the trunk and ORCHIDEE-CAN branch were run from 1850 to 1900 using CRU-NCEP climate forcing from 1901–1950 at 0.5° resolution. From 1901 until 2012, the corresponding CRU-NCEP forcing data for each year were used. Both versions used the 11-layer soil hydrology, the single-layer energy budget and the same land cover map (Poulter et al., 2014). Given that no European-wide, spatially explicit and data-derived products were found for the validation of the net carbon flux, there was no need for a carbon spin-up. For the ORCHIDEE-CAN branch, the observed tree height and basal area were compared against the simulation values at the end of 2010 (the trunk does not simulate these variables). For both the trunk and the ORCHIDEE-CAN branch, the observed GPP, evapotranspiration, effective LAI and VIS and NIR albedos were compared against monthly means between 2001 and 2010.

5.1 Allocation

In ORCHIDEE-CAN, functional relationships which vary by species and light stress are used to allocate carbon among the fine roots, foliage and sapwood. The allocation scheme largely follows Zaehle and Friend (2010), who in turn was inspired by Sitch et al. (2003). Approaches simulating allocation based on functional relationships were found to outcompete allocation schemes based on constant fractions or resource limitation (De Kauwe et al., 2014). The ability of these schemes to reproduce foliage, fine root and sapwood reported in large observational data sets (for example, Luyssaert et al., 2007) demonstrates that these schemes capture the main observed features (Zaehle and Friend, 2010). In addition, allocation schemes making use of functional relationships were also capable of simulating the observed effect of elevated CO_2 on

two mature forest ecosystems (De Kauwe et al., 2014). Despite these successes, the schemes were reported to be sensitive to their parametrization. Differences in parameters were reported to result in substantial differences in the simulated allocation. The parameters for the functional relationships used in ORCHIDEE-CAN are given in Table 4. The main conceptual difference between the allocation scheme by Zaehle and Friend (2010) and ORCHIDEE-CAN is that the latter was designed to simulate one or more diameter classes.

Given that photosynthesis is still calculated at the stand level (and thus not at the tree level) the allocation rule of Deleuze et al. (2004) was integrated in the functional allocation scheme to account for light and resource competition within a stand (see Sect. 5.6). Where the functional relationships are used to simulate carbon allocation within an individual tree of a given diameter, the rule of Deleuze and Dhote allocates carbon across the different diameter classes. The allocation rule which models the radial increment for individual trees in pure even-aged stands was successfully tested for Norway spruce and Douglas fir stands in France (Deleuze et al., 2004). A similar approach for modelling radial increment has already been implemented in a version close to the trunk of ORCHIDEE (Bellassen et al., 2010) and was able to successfully simulate stand characteristics such as height, basal area and stand diameter (Bellassen et al., 2011). This previous implementation differs from the current implementation in its time resolution (which is now daily instead of yearly), its analytical solution and the underlying allocation scheme (which is now based on functional relationships instead of resource limitation).

The aforementioned studies performed a detailed validation of the two approaches dealing with carbon allocation, which were combined in ORCHIDEE-CAN. Complementary to these studies we performed a European-wide validation of our implementation and parametrization of these well-tested schemes against a remote-sensing based map of tree height (Simard et al., 2011), upscaled eddy-covariance observations for GPP (Jung et al., 2011) and a map of basal area based on national forest inventory data (de Rigo et al., 2014). The model's ability to reproduce GPP is thought to reflect

its capacity to simulate the foliage biomass, a correct simulation of height reflects the model's capacity to simulate aboveground woody biomass and its capacity to reproduce observed basal areas suggest that the interaction of stand density and individual tree diameter are well-captured.

The new implementation and parametrization of the within-tree and within-stand allocation schemes were found to have an 91, 68 and 72 % chance that the simulations reproduced the observations for GPP, tree height and basal area for Europe, respectively (Table 7). Given that basal area and height are not available from the trunk version of ORCHIDEE, we could not compare the performance of model versions in this respect. With respect to GPP, the ORCHIDEE-CAN branch was found to outperform the trunk by 12 % and thus increased the likelihood that ORCHIDEE-CAN is an unbiased simulator of the spatial and temporal variability of GPP from 79 to 91 %. Improved performance of the ORCHIDEE-CAN branch compared to the trunk is observed for all regions in summer where the RMSE of GPP was halved from 2.5–5 to 1–2 $gC\,m^{-2}\,day^{-1}$ (Figs. 2 and 3).

Although part of the high likelihood could be due to the fact that the observed GPP was upscaled making use of similar climatologies being used as the forcings of the models, this circularity could neither have contributed to the improved performance between the trunk and the ORCHIDEE-CAN branch nor to the decrease in RMSE. The improvements are thought to be due to structural changes to the model such as allocation, hydraulic architecture and canopy structure as well as to the use of more consistent parametrization as the ORCHIDEE-CAN branch makes use of tree species rather than plant functional types.

5.2 Plant water supply

Our implementation of plant hydraulic architecture was largely based on the scheme of Hickler et al. (2006), which was tested globally and at site level. Global simulation results for actual evapotranspiration were found to reproduce available data (Baumgartner and Reichel, 1975; Henning, 1989). At the site level, the model agreed well

with the magnitude and seasonality of eddy-covariance measurements of actual evapotranspiration for 15 European forests sites (EUROFLUX), with a tendency to slightly overestimate actual evapotranspiration for 6 sites (Hickler et al., 2006).

The maximum amount of water that can be transported by a tree relies on the hydraulic architecture of the tree and therefore on the capacity of the model to simulate tree and stand dimensions as well as on the model's capacity to simulate soil water content. As an additional test, our implementation of the model was compared against the upscaled eddy-covariance measurements for GPP and actual evapotranspiration (Jung et al., 2011). The capacity to jointly reproduce GPP and actual evapotranspiration is an indicator that the model successfully reproduces the coupling between CO_2 and water exchange. Model validation showed 91 and 87 % chance (compared to 79 and 45 % for the trunk) that ORCHIDEE-CAN reproduces the upscaled GPP and actual evapotranspiration data (Table 7). The RMSE for actual evapotranspiration during summer dropped well below 1 mm day^{-1} for most regions (Fig. 2), whereas it never dropped below 1 mm day^{-1} for the trunk (Fig. 3).

5.3 Canopy structure

The canopy structure model by Haverd et al. (2012) was previously validated against ground-based LIDAR data for several test sites with varying density, structural complexity, layering and clumping (Lovell et al., 2012). Model-derived canopy gap probabilities compared with observations using a one-sample t-test were significant for 11 out of 12 test sites. We considered this result as a sufficient proof to use this canopy structure model in the ORCHIDEE-CAN branch and added to its validation by comparing the simulated canopy structure model over Europe against a remote-sensing based map of tree height (see Sect. 5.1, Simard et al., 2011) and the JRC-TIP effective LAI product (Pinty et al., 2011a). The effective LAI value expresses the capability of the canopy to intercept direct radiation, and is thus associated with the probability distribution function of the canopy gaps (Haverd et al., 2012). Thus the effective LAI contains information about the forest structure and leaf distribution of the canopy. In the ORCHIDEE-CAN

branch, canopy structure is used to calculate the albedo, roughness length, absorbed light for photosynthesis and leaf area that is coupled to the atmosphere for, e.g., transpiration and interception of precipitation.

The ORCHIDEE-CAN branch is the first branch of ORCHIDEE that makes use of an effective LAI to calculate the interaction between the canopy and the atmosphere. The LPI and RMSE of the branch, therefore, cannot be compared against the trunk. Overall, the combined implementation of the allocation scheme and the canopy structure model shows a 67 % chance to reproduce the satellite-based estimates for effective LAI. Surprisingly, effective LAI is better simulated in spring and autumn when dynamics within the canopy are substantial due to leaf on-set and senescence. For the periods when the effective LAI is expected to be most stable, i.e., summer and winter, LPI approached and frequently exceeded 1 (data not shown). Part of this shortcoming may be due to the lack of shrubs in the land cover classification. In the model, shrublands are replaced by forest and/or grasslands, likely resulting in differences between the observed and simulated canopy structure. This lapse also appears in the RMSE of effective LAI (RMSE higher than 0.8, Fig. 2).

5.4 Top of the canopy albedo

The radiation transfer model (Pinty et al., 2006) has been validated extensively against realistic complex three-dimensional canopy scenarios (Pinty et al., 2006) and as part of the RAdiation transfer Model Intercomparison (RAMI) project. The 1-D canopy radiation transfer model by Pinty et al. (2006) was demonstrated to accurately simulate both the amplitude and the angular variations of all radiant fluxes with respect to the solar zenith angle (Widlowski et al., 2011). In addition, the radiation transfer model and its effective values extracted from the JRC-TIP data set were successfully applied to a single forest site (Pinty et al., 2011c).

Previously we reported on the capacity of the radiation transfer model to simulate the effects of forest management on albedo (Otto et al., 2014). For the latter, forest properties were prescribed and the radiation transfer model was validated against top-of-

the-canopy albedo data from five observational sites. Differences in the spatial scales between the observed and simulated albedo values were accounted for by presenting the mean June albedo during 2001–2010 (Otto et al., 2014). The simulated summertime canopy albedo falls within the range of observation. However, there occurs a slight overestimation in the near-infrared wavelength band compared to the single site measurement. Too high near-infrared single scattering albedo values for pine, as obtained from the JRC-TIP product, are the most likely cause. The observed deviation is not due to a shortcoming in the model itself but reflects the difficulties the JRC-TIP has with optimizing parameter values in the absence of field observations in the specific case of sparse canopies (Otto et al., 2014).

For the spatial validation we use the white-sky albedo (VIS and NIR) from Moderate Resolution Imaging Spectroradiometer (MODIS, Schaaf et al., 2002) at 0.5° resolution (distributed in netCDF format by the Integrated Climate Data Center (ICDC, http://icdc.zmaw.de, University of Hamburg, Hamburg, Germany). Over large spatial and temporal domains the ORCHIDEE-CAN branch reproduces the observed VIS and NIR albedo and its variability; LPI for the albedo in the visible light is especially satisfying with a likelihood of 92 % for the simulations to come from the same population as the observations (Table 7). This high overall performance index, however, hides performance issues over Scandinavia and the Alps during the snow season. The RMSE for VIS and NIR albedo without snow lies around 0.05, whereas during the snow season the RMSE increases to 0.20 (VIS) and 0.18 (NIR) over these regions (Fig. 2). When the ORCHIDEE-CAN branch is coupled to an atmospheric model, however, these deviations will only have a minor effect on the climate, owing to low incoming radiation during most of the snow season, especially in Scandinavia.

Previous validation of the radiation transfer model showed that the largest discrepancies were occurring in the near-infrared domain with a snow covered background (Pinty et al., 2006). With the exception of the snow-covered season, the new albedo scheme, that relies on the simulated canopy structure, resulted in a substantial improvement of 0.05–0.15 compared to the trunk for the RMSE in both the VIS and NIR range in

Scandinavia and the Alps (Figs. 2 and 3). The European LPI-based likelihood that our model simulations come from the same populations as the MODIS albedo increased by a remarkable 11 and 23 % for, respectively, NIR and VIS albedo (from 61 and 69 % for the trunk to 72 and 92 % for the ORCHIDEE-CAN, Table 7).

Given that the parametrization of the canopy radiation transfer model used in ORCHIDEE-CAN relies on MODIS, the high likelihood may not come as a surprise. However, our implementation of the radiation transfer model also relies on the simulated absorbed light, simulated GPP, simulated allocation and simulated canopy structure (which depends on mortality and forest management). In the absence of all these processes our canopy radiation transfer model is expected to reproduce the MODIS data with a probability of 100 %. Hence, the likelihood of 72 and 92 % (for NIR and VIS, respectively) could also be interpreted as a verification of the aforementioned calculations; all calculations that determine the canopy structure reduce the reproducibility of the data by only 8–28 % (100 to 72 or 92 %).

5.5 Energy fluxes

The multilayer scheme is in the process of a detailed evaluation across a range of tests conditions (Ryder et al., 2014), and further validation across a range of sites is on-going. The scheme is able to produce within-canopy temperature and humidity profiles, and successfully simulates the in-canopy radiation distribution, as well as the separation of the canopy from the soil surface. However, in order to preserve a measure of continuity with previous evaluations of the model, the multilayer solution is here set to single layer operation mode, which includes the effects of hydraulic limitation (see Sect. 3.2) and canopy structure (see Sect. 3.3) on the energy budget.

The single-layer set-up of the multi-layer solution makes use of an improved albedo estimation and is therefore expected to better simulate the net radiation that needs to be redistributed in the canopy. This has been confirmed at a single site with a sparse canopy (Ryder et al., 2014). Furthermore, the improvements in actual evapotranspira-

tion in addition to the low RMSE (Fig. 2) are expected to be propagated in the performance of the energy budget.

5.6 Forest management strategies

Model comparison has previously demonstrated that explicitly treating thinning processes is essential to reproduce local and large scale biomass observations (Wolf et al., 2011). This finding justifies the implementation of generic approaches to forest management despite the difficulties associated with defining and quantifying forest management and its intensity (Schall and Ammer, 2013). Although the use of so-called naturalness indices, in which the current state of the forest in referenced against the potential state of the forest, has been criticised because of difficulties in defining the potential state of the forest (Schall and Ammer, 2013), such approaches were demonstrated to correctly rank different management strategies according to their intensity (Luyssaert et al., 2011).

Naturalness indices making use of only diameter and stand density or the so-called Relative Density Index (RDI) have been previously implemented at the stand-level (Fortin et al., 2012) and as well as in large scale models (Bellassen et al., 2010). This approach was shown to successfully reproduce the biomass changes during the life cycle of a forest (Bellassen et al., 2011; Fortin et al., 2012). The implementation of a forestry model based on the relative density index was reported to perform better than simple statistical models for stand-level variables such as stand density, basal area, standing volume and height (Bellassen et al., 2011). Although the performance of the model was reported as less satisfying for tree-level variables, the approach is nevertheless considered reliable to model the effects of forest management on biomass stocks of forests across a range of scales from plot to country (Bellassen et al., 2011).

The forestry model implemented in ORCHIDEE-CAN is based on the RDI approach by Bellassen et al. (2010). We complemented earlier validation of such an approach over France (Bellassen et al., 2011) by a new European-wide validation for basal area. At the European scale we verified the simulated basal area and height against ob-

served basal area from national forest inventories (de Rigo et al., 2014) and height from remote-sensing (Simard et al., 2011). With an RMSE of 3–7 for height and 7–15 for BA, and a chance of, respectively, 68 and 72 % to reproduce the data at the European scale (Table 7), our model is capable of correctly simulating the mean height and basal area but fails to capture much of the spatial variability (temporal variability was not considered because the data products were only available for one time period). This finding could be due to the simulation protocol that started in 1850 with 2 to 3 m tall trees all over Europe. A longer simulation accounting for the major historical changes in forest management such as the reforestation in the 1700 s following an all time low in the European forest cover, the start of high stand management at the expense of coppicing in the early 1800s, and the reforestation programs following World War II (Farrell et al., 2000) is expected to improve the spatial variability in tree height and basal area. Regional deviations such as those observed in the Iberian Peninsula or over the entire Mediterranean (thus including part of the Iberian Peninsula) may be due to the lack of shrubs in the land cover map and parametrization of the ORCHIDEE-CAN branch. Therefore the models simulates a higher stand density and higher basal area for regions where in reality shrubs occur.

The parametrization of the forestry module strongly depends on the national forest inventories from Spain, France, Germany and Sweden. Therefore verification against the same data contains little information about the model quality. Nevertheless, no time-dependent relationships were used in the ORCHIDEE-CAN branch thus the model's capacity to reproduce the relationship between basal area and stand age, diameter and stand age or wood volume and stand age could be considered as largely independent test of the model quality. These tests were performed over 8 bioclimatic regions of France and the ORCHIDEE-CAN branch was found to largely capture the time dependencies of basal area, diameter and wood volume (not shown).

6 Conclusions

ORCHIDEE-CAN (SVN r2290) differs from the trunk version of ORCHIDEE (SVN r2243) by the allometric-based allocation of carbon to leaf, root, wood, fruit and reserve pools; the transmittance, absorbance and reflectance of radiation within the canopy; and the vertical discretisation of the energy budget calculations. Conceptual changes towards a better process representation were made for the interaction of radiation with snow, the hydraulic architecture of plants, the representation of forest management and a numerical solution for the photosynthesis formalism of Farquhar, von Caemmerer and Berry. Furthermore, these changes were extensively linked throughout the code to improve the consistency of the model. By making use of observation-based parameters the physiological realism of the model was improved and significant reparametrization was done by introducing twelve new parameter sets that represent specific tree species or genera rather than a group of phylogenetically often unrelated species, as is the case in widely used plant functional types (PFT). As PFTs have no meaning outside the modelling community, the species level parametrization of the ORCHIDEE-CAN branch can deliver actionable information to decision-makers and forest owners on the implications of management strategies on the climate.

Model performance was tested against spatial explicit or upscaled data for basal area, tree height, canopy strucure, GPP, albedo and evapotranspiration over Europe. The tested data streams represented biogeochemical fluxes, biophysical fluxes and forest management related vegetation characteristics. Enhanced process representation in ORCHIDEE-CAN compared to the trunk version, was found to increase model performance regarding its ability to reproduce large-scale spatial patterns of all tested data streams as well as their inter-annual variability over Europe. Although this validation approach gives us confidence in the large-scale performance of the model over Europe, additional validation is recommended for other regional applications or higher resolution studies.

Code availability

The code and the run environment are open source (http://forge.ipsl.jussieu.fr/orchidee). Nevertheless readers interested in running ORCHIDEE-CAN are encouraged to contact the corresponding author for full details and latest bug fixes.

Author contributions. K. Naudts, J. Ryder, M. J. McGrath, J. Otto, and S. Luyssaert equally contributed to model development and parametrization of the OCHIDEE-CAN model.

- Developed and parametrized the ORCHIDEE-CAN model: Kim Naudts, James Ryder, Matthew J. McGrath, Juliane Otto, Sebastiaan Luyssaert, Nicolas Vuichard, Didier Solyga
- Evaluated the performance of the ORCHIDEE-CAN model: Kim Naudts, James Ryder, Juliane Otto, Matthew J. McGrath, Sebastiaan Luyssaert, Aude Valade, Yiying Chen, Fabienne Maignan
- Contributed Fortran code: Vanessa Haverd (canopy gaps), Bernard Pinty (albedo), Valentin Bellassen (forestry)
- Provided/shared observational data sets or tools for model parametrization: Hans Pretzsch, Päivi Merilä, Jens Kattge, Gerhard Bönisch, Matteo Campioli, Josep Penuelas, Detlef Schulze, Toon De Groote, Gonzalo Berhongaray, Yuan Yan, Philippe Peylin
- Developed driver data: Natasha MacBean
- Maintained and developed the run environment: Josefine Ghattas

Acknowledgements. J. Ryder, Y. Chen, M. J. McGrath, J. Otto, K. Naudts, and S. Luyssaert were funded through ERC starting grant 242564 (DOFOCO), and A. Valade was funded through ADEME (BiCaFF). ESA ECV landcover also supported this work. The research leading to these results has received funding from the European Community's Seventh Framework Programme (FP7/2007–2013) under the Grant Agreement n° 284181-TREES4FUTURE. The authors would like to thank Daniele de Rigo for providing a basal area map for Europe.

References

Amiro, B., Barr, A., Black, T., Iwashita, H., Kljun, N., Mccaughey, J., Mogenstern, K., Murayama, S., Nesic, Z., and Orchansky, A.: Carbon, energy and water fluxes at mature and disturbed forest sites, Saskatchewan, Canada, Agr. Forest Meteorol., 136, 237–251, doi:10.1016/j.agrformet.2004.11.012, 2006a. 8568

Amiro, B., Orchansky, A., Barr, A., Black, T., Chambers, S., Chapin III, F., Goulden, M., Litvak, M., Liu, H., McCaughey, J., McMillan, A., and Randerson, J.: The effect of post-fire stand age on the boreal forest energy balance, Agr. Forest Meteorol., 140, 41–50, doi:10.1016/j.agrformet.2006.02.014, 2006b. 8568

Amthor, J. S.: The role of maintenance respiration in plant growth, Plant Cell Environ., 7, 561–569, doi:10.1111/1365-3040.ep11591833, 1984. 8577

Aranda, I., Gil, L., and Pardos, J.: Seasonal changes in apparent hydraulic conductance and their implications for water use of European beech (*Fagus sylvatica* L.) and sessile oak [*Quercus petraea* (Matt.) Liebl] in South Europe, Plant Ecol., 179, 155–167, doi:10.1007/s11258-004-7007-1, 2005. 8639

Arneth, A., Kelliher, F. M., Bauer, G., Hollinger, D. Y., Byers, J. N., Hunt, J. E., Seveny, T. M. M. C., Ziegler, W., Vygodskaya, N. N., Milukova, I., Sogachov, A., Varlagin, A., and Schulze, E.-D.: Environmental regulation of xylem sap flow and total conductance of Larix gmelinii trees in eastern Siberia, Tree Physiol., 16, 247–255, 1996. 8639

Bala, G., Caldeira, K., Wickett, M., Phillips, T. J., Lobell, D. B., Delire, C., and Mirin, A.: Combined climate and carbon-cycle effects of large-scale deforestation, P. Natl. Acad. Sci. USA, 104, 6550–5, doi:10.1073/pnas.0608998104, 2007. 8568

Baldocchi, D.: A multi-layer model for estimating sulfur dioxide deposition to a deciduous oak forest canopy, Atmos. Environ., 22, 869–884, doi:10.1016/0004-6981(88)90264-8, 1988. 8574, 8590

Ball, J. T., Woodrow, I. E., and Berry, J. A.: A model predicting stomatal conductance and its contribution to the control of photosynthesis under different environmental conditions, in: Progress in Photosynthesis Research, edited by: Biggins, J. and Nijhoff, M., Martinus-Nijhoff Publishers, Dordrecht, the Netherlands, 221–224, 1987. 8590

Bartelink, H. H.: Allometric relationships for biomass and leaf area of beech (*Fagus sylvatica* L), Ann. For. Sci., 54, 39–50, 1997. 8637

Baumgartner, A. and Reichel, E.: Die Weltwasserbilanz, R. Oldenburg Verlag, Munich, 1975. 8606

Bellassen, V., Le Maire, G., Dhôte, J., Ciais, P., and Viovy, N.: Modelling forest management within a global vegetation model Part 1: Model structure and general behaviour, Ecol. Model., 221, 2458–2474, doi:10.1016/j.ecolmodel.2010.07.008, 2010. 8571, 8576, 8593, 8605, 8611, 8633

Bellassen, V., Le Maire, G., Guin, O., Dhôte, J., Ciais, P., and Viovy, N.: Modelling forest management within a global vegetation model Part 2: Model validation from a tree to a continental scale, Ecol. Model., 222, 57–75, doi:10.1016/j.ecolmodel.2010.08.038, 2011. 8605, 8611

Bellprat, O., Kotlarski, S., Lüthi, D., and Schär, C.: Objective calibration of regional climate models, J. Geophys. Res., 117, D23115, doi:10.1029/2012JD018262, 2012. 8603

Berthier, S., Kokutse, A., Stokes, A., and Fourcaud, T.: Irregular Heartwood formation in maritime pine (*Pinus pinaster* ait): consequences for biomechanical and hydraulic tree functioning, Ann. Bot.-London, 87, 19–25, doi:10.1006/anbo.2000.1290, 2001. 8637

Best, M. J., Beljaars, A., Polcher, J., and Viterbo, P.: A proposed structure for coupling tiled surfaces with the planetary boundary layer, J. Hydrometeorol., 5, 1271–1278, doi:10.1175/JHM-382.1, 2004. 8574

Betts, R. A.: Offset of the potential carbon sink from boreal forestation by decreases in surface albedo, Nature, 408, 187–90, doi:10.1038/35041545, 2000. 8568

Björklund, L.: Identifying Heartwood-rich stands or stems of *pinus sylvestris* by using inventory data, Silva Fenn., 33, 119–129, 1999. 8637

Bonan, G. B.: Forests and climate change: forcings, feedbacks, and the climate benefits of forests, Science, 320, 1444–1449, doi:10.1126/science.1155121, 2008. 8569

Bonan, G. B., Levis, S., Sitch, S., Vertenstein, M., and Oleson, K. W.: A dynamic global vegetation model for use with climate models: concepts and description of simulated vegetation dynamics, Glob. Change Biol., 9, 1543–1566, doi:10.1046/j.1365-2486.2003.00681.x, 2003. 8569

Bonan, G. B., Williams, M., Fisher, R. A., and Oleson, K. W.: Modeling stomatal conductance in the earth system: linking leaf water-use efficiency and water transport along the soil–plant–atmosphere continuum, Geosci. Model Dev., 7, 2193–2222, doi:10.5194/gmd-7-2193-2014, 2014. 8581

Botta, A., Viovy, N., Ciais, P., Friedlingstein, P., and Monfray, P.: A global prognostic scheme of leaf onset using satellite data, Glob. Change Biol., 6, 709–725, doi:10.1046/j.1365-2486.2000.00362.x, 2000. 8633

Bréda, N. and Granier, A.: Intra- and interannual variations of transpiration, leaf area index and radial growth of a sessile oak stand (*Quercus petraea*), Ann. For. Sci., 53, 521–536, 1996. 8637

Brunner, I., Bakker, M. R., Björk, R. G., Hirano, Y., Lukac, M., Aranda, X., Børja, I., Eldhuset, T. D., Helmisaari, H. S., Jourdan, C., Konôpka, B., López, B. C., Miguel Pérez, C., Persson, H., and Ostonen, I.: Fine-root turnover rates of European forests revisited: an analysis of data from sequential coring and ingrowth cores, Plant Soil, 362, 357–372, doi:10.1007/s11104-012-1313-5, 2013. 8638

Brus, D., Hengeveld, G., Walvoort, J., Goedhart, P., Heidema, A., Nabuurs, G., and Gunia, K.: Statistical mapping of tree species over Europe, Eur. J. Forest Res., 131, 145–157, 2012. 8595, 8600

Campioli, M., Vicca, S., Luyssaert, S., Bilcke, J., Ceschia, E., Chapin III, F., Ciais, P., Fernández-Martínez, M., Malhi, Y., Obersteiner, M., Olefeldt, D., Papale, D., Piao, S., Peñuelas, J., Sullivan, P., Wang, X., Zenone, T., and Janssens, I.: Management improves the efficiency of biomass production of global terrestrial ecosystems, 2014, in preperation. 8597

Carsel, R. F. and Parrish, R. S.: Developing joint probability distributions of soil water retention characteristics, Water Resour. Res., 24, 755–769, doi:10.1029/WR024i005p00755, 1988. 8640

Choat, B., Jansen, S., Brodribb, T. J., Cochard, H., Delzon, S., Bhaskar, R., Bucci, S. J., Feild, T. S., Gleason, S. M., Hacke, U. G., Jacobsen, A. L., Lens, F., Maherali, H., Martínez-Vilalta, J., Mayr, S., Mencuccini, M., Mitchell, P. J., Nardini, A., Pittermann, J., Pratt, R. B., Sperry, J. S., Westoby, M., Wright, I. J., and Zanne, A. E.: Global convergence in the vulnerability of forests to drought, Nature, 491, 752–755, doi:10.1038/nature11688, 2012. 8639

Cochard, H.: Vulnerability of several conifers to air embolism, Tree Physiol., 11, 73–83, doi:10.1093/treephys/11.1.73, 1992. 8639

Cochard, H., Martin, R., Gross, P., and Bogeat-Triboulot, M.: Temperature effects on hydraulic conductance and water relations of *Quercus robur* L., J. Exp. Bot., 51, 1255–1259, 2000. 8584, 8639

Collatz, G., Ribas-Carbo, M., and Berry, J.: Coupled photosynthesis-stomatal conductance model for leaves of C4 plants, Aust. J. Plant Physiol., 19, 519–538, 1992. 8632

Corcuera, L., Camarero, J. J., and Gil-Pelegrin, E.: Effects of a severe drought on *Quercus ilex* radial growth and xylem anatomy, Trees-Struct. Func., 18, 83–92, doi:10.1007/s00468-003-0284-9, 2004. 8639

Cox, P. M., Betts, R. A., Bunton, C. B., Essery, R. L. H., Rowntree, P. R., and Smith, J.: The impact of new land surface physics on the GCM simulation of climate and climate sensitivity, Clim. Dynam., 15, 183–203, doi:10.1007/s003820050276, 1999. 8569

David, T., Ferreira, M., Cohen, S., Pereira, J., and David, J.: Constraints on transpiration from an evergreen oak tree in southern Portugal, Agr. Forest Meteorol., 122, 193–205, doi:10.1016/j.agrformet.2003.09.014, 2004. 8637

Davin, E. L., de Noblet-Ducoudré, N., and Friedlingstein, P.: Impact of land cover change on surface climate: relevance of the radiative forcing concept, Geophys. Res. Lett., 34, L13702, doi:10.1029/2007GL029678, 2007. 8568

De Kauwe, M. G., Medlyn, B. E., Zaehle, S., Walker, A. P., Dietze, M. C., Hickler, T., Jain, A. K., Luo, Y., Parton, W. J., Prentice, I. C., Smith, B., Thornton, P. E., Wang, S., Wang, Y.-P., Wårlind, D., Weng, E., Crous, K. Y., Ellsworth, D. S., Hanson, P. J., Seok Kim, H., Warren, J. M., Oren, R., and Norby, R. J.: Forest water use and water use efficiency at elevated CO_2: a model-data intercomparison at two contrasting temperate forest FACE sites., Glob. Change Biol., 19, 1759–1779, doi:10.1111/gcb.12164, 2013. 8581

De Kauwe, M. G., Medlyn, B. E., Zaehle, S., Walker, A. P., Dietze, M. C., Wang, Y.-P., Luo, Y., Jain, A. K., El-Masri, B., Hickler, T., Wårlind, D., Weng, E., Parton, W. J., Thornton, P. E., Wang, S., Prentice, I. C., Asao, S., Smith, B., McCarthy, H. R., Iversen, C. M., Hanson, P. J., Warren, J. M., Oren, R., and Norby, R. J.: Where does the carbon go? A model-data intercomparison of vegetation carbon allocation and turnover processes at two temperate forest free-air CO_2 enrichment sites, New Phytol., 203, 883–899, doi:10.1111/nph.12847, 2014. 8604, 8605

de Noblet-Ducoudré, N., Boisier, J.-P., Pitman, A., Bonan, G. B., Brovkin, V., Cruz, F., Delire, C., Gayler, V., van den Hurk, B. J. J. M., Lawrence, P. J., van der Molen, M. K., Müller, C., Reick, C. H., Strengers, B. J., and Voldoire, A.: Determining robust impacts of land-use-induced land cover changes on surface climate over North America and Eurasia: results from the first set of LUCID experiments, J. Climate, 25, 3261–3281, doi:10.1175/JCLI-D-11-00338.1, 2012. 8589

de Rigo, D., Caudullo, G., Busetto, L., and San Miguel, J.: Supporting EFSA assessment of the EU environmental suitability for exotic forestry pests: final report, Tech. rep., EFSA Supporting publications, Joint Research Centre, Ispra, Italy, 2014. 8604, 8605, 8612

de Rosnay, P.: Impact of a physically based soil water flow and soil-plant interaction representation for modeling large-scale land surface processes, J. Geophys. Res., 107, 4118, doi:10.1029/2001JD000634, 2002. 8572

de Rosnay, P. and Polcher, J.: Modelling root water uptake in a complex land surface scheme coupled to a GCM, Hydrol. Earth Syst. Sci., 2, 239–255, doi:10.5194/hess-2-239-1998, 1998. 8570

Deleuze, C., Pain, O., Dhôte, J.-F., and Hervé, J.-C.: A flexible radial increment model for individual trees in pure even-aged stands, Ann. For. Sci., 61, 327–335, doi:10.1051/forest:2004026, 2004. 8571, 8572, 8580, 8605, 8633

Dickinson, R., Henderson-Sellers, A., Kennedy, P., and Wilson, M.: Biosphere-Atmosphere Transfer Scheme (BATS) for the NCAR Community Climate Model, Tech. Rep. December, 1986. 8574

Dixon, R. K., Solomon, A. M., Brown, S., Houghton, R. A., Trexier, M. C., and Wisniewski, J.: Carbon pools and flux of global forest ecosystems, Science, 263, 185–90, doi:10.1126/science.263.5144.185, 1994. 8568

d'Orgeval, T., Polcher, J., and de Rosnay, P.: Sensitivity of the West African hydrological cycle in ORCHIDEE to infiltration processes, Hydrol. Earth Syst. Sci., 12, 1387–1401, doi:10.5194/hess-12-1387-2008, 2008. 8632

Ducoudré, N. I., Laval, K., and Perrier, A.: SECHIBA, a new set of parametrizations of the hydrologic exchanges at the land-atmosphere interface within the LMD atmospheric general circulation model, J. Climate, 6, 248–273, 1993. 8570

Dufresne, J. and Ghattas, J.: Description du schéma de la couche limite turbulente et l' interface avec la surface planetaire dans LMDZ, Technical, 1–19, available at: http://lmdz.lmd.jussieu.fr/developpeurs/notes-techniques/ressources/pbl_surface.pdf (last access: 2 December 2014), 2001. 8632

Farquhar, G. D., von Caemmerer, S., and Berry, J. A.: A biochemical model of photosynthetic CO_2 assimilation in leaves of C3 species, Planta, 149, 78–90, doi:10.1007/BF00386231, 1980. 8591, 8592, 8600, 8632

Farrell, E. P., Führer, E., Ryan, D., Andersson, F., Hüttl, R., and Piussi, P.: European forest ecosystems: building the future on the legacy of the past, Forest Ecol. Manag., 132, 5–20, doi:10.1016/S0378-1127(00)00375-3, 2000. 8612

Fichot, R., Barigah, T. S., Chamaillard, S., Le Thiec, D., Laurans, F., Cochard, H., and Brignolas, F.: Common trade-offs between xylem resistance to cavitation and other physiological traits do not hold among unrelated *Populus deltoides* × *Populus nigra* hybrids, Plant Cell Environ., 33, 1553–1568, doi:10.1111/j.1365-3040.2010.02164.x, 2010. 8639

Fichot, R., Chamaillard, S., Depardieu, C., Le Thiec, D., Cochard, H., Barigah, T. S., and Brignolas, F.: Hydraulic efficiency and coordination with xylem resistance to cavitation, leaf function, and growth performance among eight unrelated *Populus deltoides* × *Populus nigra* hybrids, J. Exp. Bot., 62, 2093–2106, doi:10.1093/jxb/erq415, 2011. 8639

Flexas, J., Bota, J., Galmés, J., Medrano, H., and Ribas-Carbó, M.: Keeping a positive carbon balance under adverse conditions: responses of photosynthesis and respiration to water stress, Physiologia Plantarum, 127, 343–352, doi:10.1111/j.1399-3054.2006.00621.x, 2006. 8572

Fortin, M., Ningre, F., Robert, N., and Mothe, F.: Quantifying the impact of forest management on the carbon balance of the forest-wood product chain: a case study applied to even-aged oak stands in France, Forest Ecol. Manag., 279, 176–188, doi:10.1016/j.foreco.2012.05.031, 2012. 8611

Friedlingstein, P., Joel, G., Field, C. B., and Fung, I. Y.: Toward an allocation scheme for global terrestrial carbon models, Glob. Change Biol., 5, 755–770, doi:10.1046/j.1365-2486.1999.00269.x, 1999. 8633

Gaspar, M., Louzada, J. L., Aguiar, A., and Almeida, M. H.: Genetic correlations between wood quality traits of *Pinus pinaster* Ait., Ann. For. Sci., 65, 703–703, doi:10.1051/forest:2008054, 2008. 8637

Gebauer, T., Horna, V., and Leuschner, C.: Variability in radial sap flux density patterns and sapwood area among seven co-occurring temperate broad-leaved tree species, Tree Physiol., 28, 1821–1830, doi:10.1093/treephys/28.12.1821, 2008. 8637

Gimmi, U., Poulter, B., Wolf, A., Portner, H., Weber, P., and Bürgi, M.: Soil carbon pools in Swiss forests show legacy effects from historic forest litter raking, Landscape Ecol., 28, 835–846, doi:10.1007/s10980-012-9778-4, 2012. 8576

Gould, P. J. and Harrington, C. A.: Extending sapwood – leaf area relationships from stems to roots in Coast Douglas-fir, Ann. For. Sci., 65, 802–802, doi:10.1051/forest:2008067, 2008. 8637

Gu, L.: Longwave radiative transfer in plant canopies, PhD thesis, University of Virginia, Virginia, 1988. 8591

Gu, L., Shugart, H. H., Fuentes, J. D., Black, T., and Shewchuk, S. R.: Micrometeorology, biophysical exchanges and NEE decomposition in a two-story boreal forest – development and test of an integrated model, Agr. Forest Meteorol., 94, 123–148, doi:10.1016/S0168-1923(99)00006-4, 1999. 8591

Hacke, U. and Sauter, J. J.: Vulnerability of xylem to embolism in relation to leaf water potential and stomatal conductance in *Fagus sylvatica f. purpurea* and *Populus balsamifera*, J. Experiment. Botany, 46, 1177–1183, 1995. 8639

Haverd, V., Lovell, J., Cuntz, M., Jupp, D., Newnham, G., and Sea, W.: The Canopy Semianalytic Pgap And Radiative Transfer (CanSPART) model: formulation and application, Agr. Forest Meteorol., 160, 14–35, doi:10.1016/j.agrformet.2012.01.018, 2012. 8573, 8585, 8607

Henning, D.: Atlas of the surface heat balance of the continents, Gebrüder Borntträger, Berlin, Stuttgart, 1989. 8606

Hickler, T., Prentice, I. C., Smith, B., Sykes, M. T., and Zaehle, S.: Implementing plant hydraulic architecture within the LPJ dynamic global vegetation model, Global Ecol. Biogeogr., 15, 567–577, doi:10.1111/j.1466-822X.2006.00254.x 2006. 8572, 8582, 8598, 8606, 8607, 8639

Hourdin, F.: A new representation of the absorption by the CO 2 15-µm band for a Martian general circulation model, J. Geophys. Res., 97, 18319, doi:10.1029/92JE01985, 1992. 8632

Jackson, R. B., Jobbágy, E. G., Avissar, R., Roy, S. B., Barrett, D. J., Cook, C. W., Farley, K. A., le Maitre, D. C., McCarl, B. A., and Murray, B. C.: Trading water for carbon with biological carbon sequestration, Science, 310, 1944–1947, doi:10.1126/science.1119282, 2005. 8568

Jenkins, J. C., Chojnacky, D. C., Heath, L. S., and Birdsey, R. A.: National-scale biomass estimators for United States tree species, Forest Sci., 49, 12–35, 2003. 8637

Jiménez, C., Prigent, C., Mueller, B., Seneviratne, S. I., McCabe, M. F., Wood, E. F., Rossow, W. B., Balsamo, G., Betts, A. K., Dirmeyer, P. A., Fisher, J. B., Jung, M., Kanamitsu, M., Reichle, R. H., Reichstein, M., Rodell, M., Sheffield, J., Tu, K., and Wang, K.: Global intercomparison of 12 land surface heat flux estimates, J. Geophys. Res., 116, D02102, doi:10.1029/2010JD014545, 2011. 8589

Jung, M., Reichstein, M., Margolis, H. A., Cescatti, A., Richardson, A. D., Arain, M.A., Arneth, A., Bernhofer, C., Bonal, D., Chen, J., Gianelle, D., Gobron, N., Kiely, G., Kutsch, W., Lasslop, G., Law, B. E., Lindroth, A., Merbold, L., Montagnani, L., Moors, E.J., Papale, D., Sottocornola, M., Vaccari, F., and Williams, C.: Global patterns of land-atmosphere fluxes of carbon dioxide, latent heat, and sensible heat derived from eddy covariance, satellite, and meteorological observations, J. Geophys. Res.-Biogeosci., 116, doi:10.1029/2010JG001566, 2011. 8604, 8605, 8607

Kattge, J. and Knorr, W.: Temperature acclimation in a biochemical model of photosynthesis: a reanalysis of data from 36 species, Plant Cell Environ., 30, 1176–1190, doi:10.1111/j.1365-3040.2007.01690.x, 2007. 8575, 8600

Kattge, J., Díaz, S., Lavorel, S., Prentice, I. C., Leadley, P., Bönisch, G., Garnier, E., Westoby, M., Reich, P. B., Wright, I. J., Cornelissen, J. H. C., Violle, C., Harrison, S. P., Van Bodegom, P. M., Reichstein, M., Enquist, B. J., Soudzilovskaia, N. A., Ackerly, D. D., Anand, M., Atkin, O., Bahn, M., Baker, T. R., Baldocchi, D., Bekker, R., Blanco, C. C., Blonder, B., Bond, W. J., Bradstock, R., Bunker, D. E., Casanoves, F., Cavender-Bares, J., Chambers, J. Q., Chapin III, F. S., Chave, J., Coomes, D., Cornwell, W. K., Craine, J. M., Dobrin, B. H., Duarte, L., Durka, W., Elser, J., Esser, G., Estiarte, M., Fagan, W. F., Fang, J., Fernández-Méndez, F., Fidelis, A., Finegan, B., Flores, O., Ford, H., Frank, D., Freschet, G. T., Fyllas, N. M., Gallagher, R. V., Green, W. A., Gutierrez, A. G., Hickler, T., Higgins, S. I., Hodgson, J. G., Jalili, A., Jansen, S., Joly, C. A., Kerkhoff, A. J., Kirkup, D., Kitajima, K., Kleyer, M., Klotz, S., Knops, J. M. H., Kramer, K., Kühn, I., Kurokawa, H., Laughlin, D., Lee, T. D., Leishman, M., Lens, F., Lenz, T., Lewis, S. L., Lloyd, J., Llusià, J., Louault, F., Ma, S., Mahecha, M. D., Manning, P., Massad, T., Medlyn, B. E., Messier, J., Moles, A. T., Müller, S. C., Nadrowski, K., Naeem, S., Niinemets, Ü., Nöllert, S., Nüske, A., Ogaya, R., Oleksyn, J., Onipchenko, V. G., Onoda, Y., Ordoñez, J., Overbeck, G., Ozinga, W. A., Patiño, S., Paula, S., Pausas, J. G., Peñuelas, J., Phillips, O. L., Pillar, V., Poorter, H., Poorter, L., Poschlod, P., Prinzing, A., Proulx, R., Rammig, A., Reinsch, S., Reu, B., Sack, L., Salgado-Negret, B., Sardans, J., Shiodera, S., Shipley, B., Siefert, A., Sosinski, E., Soussana, J.-F., Swaine, E., Swenson, N., Thompson, K., Thornton, P., Waldram, M., Weiher, E., White, M., White, S., Wright, S. J., Yguel, B., Zaehle, S., Zanne, A. E., and Wirth, C.: TRY – a global database of plant traits, Glob. Change Biol., 17, 2905–2935, doi:10.1111/j.1365-2486.2011.02451.x, 2011. 8575, 8600

Kira, T., Ogawa, H., and Sakazaki, N.: Intraspecific competition among higher plants. I. Competition-yield-density interrelationship in regularly dispersed populations, Journal of the Institute of Polytechnics (Osaka University), 4, 1–16, 1953. 8602

Knapic, S., Louzada, J. L., Leal, S., and Pereira, H.: Within-tree and between-tree variation of wood density components in cork oak trees in two sites in Portugal, Forestry, 81, 465–473, doi:10.1093/forestry/cpn012, 2008. 8637

Krinner, G., Nicolas, V., de Noblet-Ducoudre, N., Ogée, J., Polcher, J., Friedlingstein, P., Ciais, P., Sitch, S., and Prentice, I.: A dynamic global vegetation model for studies of the coupled atmosphere-biosphere system, Global Biogeochem. Cy., 19, GB1015, doi:10.1029/2003GB002199, 2005. 8569, 8570

Lardy, R., Bellocchi, G., and Soussana, J.-F.: A new method to determine soil organic carbon equilibrium, Environ. Modell. Softw., 26, 759–1763, doi:10.1016/j.envsoft.2011.05.016, 2011. 8571

Limousin, J.-M., Rambal, S., Ourcival, J.-M., Rodríguez-Calcerrada, J., Pérez-Ramos, I. M., Rodríguez-Cortina, R., Misson, L., and Joffre, R.: Morphological and phenological shoot plasticity in a Mediterranean evergreen oak facing long-term increased drought, Oecologia, 169, 565–577, doi:10.1007/s00442-011-2221-8, 2012. 8637, 8639

Longuetaud, F., Mothe, F., Leban, J.-M., and Mäkelä, A.: *Picea abies* sapwood width: variations within and between trees, Scand. J. Forest Res., 21, 41–53, doi:10.1080/02827580500518632, 2006. 8637

Lovell, J., Haverd, V., Jupp, D., and Newnham, G.: The Canopy Semi-analytic Pgap And Radiative Transfer (CanSPART) model: validation using ground based lidar, Agr. Forest Meteorol., 158–159, 1–12, doi:10.1016/j.agrformet.2012.01.020, 2012. 8607

Luyssaert, S., Inglima, I., Jung, M., Richardson, A. D., Reichstein, M., Papale, D., Piao, S. L., Schulze, E. D., Wingate, L., Matteucci, G., Aragao, L., Aubinet, M., Beer, C., Bernhofer, C., Black, K. G., Bonal, D., Bonnefond, J. M., Chambers, J., Ciais, P., Cook, B., Davis, K. J., Dolman, A. J., Gielen, B., Goulden, M., Grace, J., Granier, A., Grelle, A., Griffis, T., Grünwald, T., Guidolotti, G., Hanson, P. J., Harding, R., Hollinger, D. Y., Hutyra, L. R., Kolari, P., Kruijt, B., Kutsch, W., Lagergren, F., Laurila, T., Law, B., Le Maire, G., Lindroth, A., Loustau, D., Malhi, Y., Mateus, J., Migliavacca, M., Misson, L., Montagnani, L., Moncrieff, J., Moors, E., Munger, J. W., Nikinmaa, E., Ollinger, S. V., Pita, G., Rebmann, C., Roupsard, O., Saigusa, N., Sanz, M. J., Seufert, G., Sierra, C., Smith, M. L., Tang, J., Valentini, R., Vesala, T., and Janssens, I. A.: CO_2 balance of boreal, temperate, and tropical forests

derived from a global database, Glob. Change Biol., 13, 2509–2537, doi:10.1111/j.1365-2486.2007.01439.x, 2007. 8604

Luyssaert, S., Hessenmöller, D., von Lüpke, N., Kaiser, S., and Schulze, E. D.: Quantifying land use and disturbance intensity in forestry, based on the self-thinning relationship, Ecol. Appl., 21, 3272–3284, doi:10.1890/10-2395.1, 2011. 8611

Luyssaert, S., Jammet, M., Stoy, P., Estel, S., Pongratz, J., Ceschia, E., Churkina, G., Don, A., Erb, K., Ferlicoq, M., Gielen, B., Grünwald, T., Houghton, R., Klumpp, K., Knohl, A., Kolb, T., Kuemmerle, T., Laurila, T., Lohila, A., Loustau, D., McGrath, M., Meyfroidt, P., Moors, E., Naudts, K., Novick, K., Otto, J., Pilegaard, K., Pio, C., Rambal, S., Rebmann, C., Ryder, J., Suyker, A., Varlagin, A., Wattenbach, M., and Dolman, A.: Land management and land-cover change have impacts of similar magnitude on surface temperature, Nature Climate Change, 4, 389–393, doi:10.1038/NCLIMATE2196, 2014. 8568

MacBean, N., Maignan, F., Peylin,P., Bacour, C., and Ciais, P.: Using satellite data to improve the leaf phenology of a global Land Surface Model, in preparation, 2014. 8596

Magnani, F., Mencuccini, M., and Grace, J.: Age-related decline in stand productivity: the role of structural acclimation under hydraulic constraints, Plant Cell Environ., 23, 251–263, 2000. 8579, 8583, 8639

Manzoni, S., Vico, G., Katul, G., Palmroth, S., Jackson, R. B., and Porporato, A.: Hydraulic limits on maximum plant transpiration and the emergence of the safety-efficiency trade-off, New Phytol., 198, 169–78, doi:10.1111/nph.12126, 2013. 8639

Margolis, H., Oren, R., Whitehead, D., and Kaufmann, M.: Leaf area dynamics of conifer forests, in: Ecophysiology of Coniferous Forests, edited by: Smith, W. and Hinckley, T., Academic Press, San Diego, 181–223, 1995. 8637

Martin, J. G., Kloeppel, B. D., Schaefer, T. L., Kimbler, D. L., and Mcnuity, S. G.: Aboveground biomass and nitrogen allocation of ten deciduous southern Appalachian tree species, Can. J. Forest Res., 28, 1648–1659, 1998. 8637

Martin, M. P., Cordier, S., Balesdent, J., and Arrouays, D.: Periodic solutions for soil carbon dynamics equilibriums with time-varying forcing variables, Ecol. Model., 204, 523–530, doi:10.1016/j.ecolmodel.2006.12.030, 2007. 8571

Martinez-Vilalta, J., Sala, A., and Pinol, J.: The hydraulic architecture of Pinaceae – a review, Plant Ecol., 171, 3–13, 2004. 8639

Massman, W. and Weil, J.: An analytical one-dimensional second-order closure model of turbulence statistics and the Lagrangian time scale within and above plant canopies of arbitrary structure, Bound.-Lay. Meteorol., 91, 81–107, 1999. 8591
McCree, K.: Equation for the rate of dark respiration of white clover as a function of dry weight, photosynthesis rate and temperature, Crop Sci., 14, 509–514, 1974.
McDowell, N., Barnard, H., Bond, B., Hinckley, T., Hubbard, R., Ishii, H., Köstner, B., Magnani, F., Marshall, J., Meinzer, F., Phillips, N., Ryan, M., and Whitehead, D.: The relationship between tree height and leaf area: sapwood area ratio, Oecologia, 132, 12–20, doi:10.1007/s00442-002-0904-x, 2002. 8597, 8637
McGrath, M. J., Pinty, B., Ryder, J., Otto, J., and Luyssaert, S.: A multilevel canopy radiative transfer scheme based on a domain-averaged structure factor, in preperation, 2014. 8573, 8587, 8588
Meador, W. E. and Weaver, W. R.: Two-stream approximations to radiative transfer in planetary atmospheres: a unified description of existing methods and a new improvement, J. Atmos. Sci., 37, 630–643, doi:10.1175/1520-0469(1980)037<0630:TSATRT>2.0.CO;2, 1980. 8586
Meadows, J. S. and Hodges, J. D.: Sapwood area as an estimator of leaf area and foliar weight in cherrybark oak and green ash, Forest Sci., 48, 69–76, 2002. 8637
Medlyn, B. E., Dreyer, E., Ellsworth, D., Forstreuter, M., Harley, P. C., Kirschbaum, M. U. F., Le Roux, X., Montpied, P., Strassemeyer, J., Walcroft, A., Wang, K., and Loustau, D.: Temperature response of parameters of a biochemically based model of photosynthesis. II. A review of experimental data, Plant Cell Environ., 25, 1167–1179, doi:10.1046/j.1365-3040.2002.00891.x, 2002. 8600
Mencuccini, M. and Bonosi, L.: Leaf/sapwood area ratios in Scots pine show acclimation across Europe, Can. J. Forest Res., 31, 442–456, doi:10.1139/cjfr-31-3-442, 2001. 8637
Murphy, J. M., Sexton, D. M. H., Barnett, D. N., Jones, G. S., Webb, M. J., Collins, M., and Stainforth, D. A.: Quantification of modelling uncertainties in a large ensemble of climate change simulations, Nature, 430, 768–771, doi:10.1038/nature02771 2004. 8603
Novick, K., Oren, R., Stoy, P., Juang, J.-Y., Siqueira, M., and Katul, G.: The relationship between reference canopy conductance and simplified hydraulic architecture, Adv. Water Resour., 32, 809–819, doi:10.1016/j.advwatres.2009.02.004, 2009. 8597, 8637
Ogee, J., Brunet, Y., Loustau, D., Berbigier, P., and Delzon, S.: MuSICA, a CO_2, water and energy multilayer, multileaf pine forest model: evaluation from hourly to yearly time scales and

sensitivity analysis, Glob. Change Biol., 9, 697–717, doi:10.1046/j.1365-2486.2003.00628.x, 2003. 8574
Olson, J., Watts, J., and Allison, L.: Carbon in live vegetation of major world ecosystems, Tech. rep., Oak Ridge National Laboratory, ORNL-82, Oak Ridge, TN, 1983. 8595
Otto, J., Berveiller, D., Bréon, F.-M., Delpierre, N., Geppert, G., Granier, A., Jans, W., Knohl, A., Kuusk, A., Longdoz, B., Moors, E., Mund, M., Pinty, B., Schelhaas, M.-J., and Luyssaert, S.: Forest summer albedo is sensitive to species and thinning: how should we account for this in Earth system models?, Biogeosciences, 11, 2411–2427, doi:10.5194/bg-11-2411-2014, 2014. 8608, 8609
Parton, W. J., Stewart, J. W. B., and Cole, C. V.: Dynamics of C, N, P and S in grassland soils: a model, Biogeochemistry, 5, 109–131, doi:10.1007/BF02180320, 1988. 8633
Pataki, D. E., Alig, R. J., Fung, A. S., Golubiewski, N. E., Kennedy, C. A., Mcpherson, E. G., Nowak, D. J., Pouyat, R. V., and Romero Lankao, P.: Urban ecosystems and the North American carbon cycle, Glob. Change Biol., 12, 2092–2102, doi:10.1111/j.1365-2486.2006.01242.x, 2006. 8597
Pielke, R. A., Marland, G., Betts, R. A., Chase, T. N., Eastman, J. L., Niles, J. O., Niyogi, D. D. S., and Running, S. W.: The influence of land-use change and landscape dynamics on the climate system: relevance to climate-change policy beyond the radiative effect of greenhouse gases, Philos. T. R. Soc. A, 360, 1705–1719, doi:10.1098/rsta.2002.1027, 2002. 8568
Pinty, B.: Synergy between 1-D and 3-D radiation transfer models to retrieve vegetation canopy properties from remote sensing data, J. Geophys. Res., 109, D21205, doi:10.1029/2004JD005214, 2004. 8587
Pinty, B., Lavergne, T., Dickinson, R. E., Widlowski, J.-L., Gobron, N., and Verstraete, M. M.: Simplifying the interaction of land surfaces with radiation for relating remote sensing products to climate models, J. Geophys. Res., 111, D02116, doi:10.1029/2005JD005952, 2006. 8573, 8574, 8586, 8587, 8588, 8599, 8608, 8609
Pinty, B., Lavergne, T., Voßbeck, M., Kaminski, T., Aussedat, O., Giering, R., Gobron, N., Taberner, M., Verstraete, M. M., and Widlowski, J.-L.: Retrieving surface parameters for climate models from Moderate Resolution Imaging Spectroradiometer (MODIS)-Multiangle Imaging Spectroradiometer (MISR) albedo products, J. Geophys. Res., 112, D10116, doi:10.1029/2006JD008105, 2007. 8599, 8640
Pinty, B., Andredakis, I., Clerici, M., Kaminski, T., Taberner, M., Verstraete, M. M., Gobron, N., Plummer, S., and Widlowski, J.-L.: Exploiting the MODIS albedos with the Two-stream In-

version Package (JRC-TIP): 1. effective leaf area index, vegetation, and soil properties, J. Geophys. Res., 116, D09105, doi:10.1029/2010JD015372, 2011a. 8596, 8599, 8604, 8607
Pinty, B., Clerici, M., Andredakis, I., Kaminski, T., Taberner, M., Verstraete, M. M., Gobron, N., Plummer, S., and Widlowski, J.-L.: Exploiting the MODIS albedos with the Two-stream Inversion Package (JRC-TIP): 2. Fractions of transmitted and absorbed fluxes in the vegetation and soil layers, J. Geophys. Res., 116, D09106, doi:10.1029/2010JD015373, 2011b. 8596, 8599
Pinty, B., Jung, M., Kaminski, T., Lavergne, T., Mund, M., Plummer, S., Thomas, E., and Widlowski, J.-L.: Evaluation of the JRC-TIP 0.01° products over a mid-latitude deciduous forest site, Remote Sens. Environ., 115, 3567–3581, doi:10.1016/j.rse.2011.08.018, 2011c. 8608
Pitman, A. J., de Noblet-Ducoudré, N., Cruz, F. T., Davin, E. L., Bonan, G. B., Brovkin, V., Claussen, M., Delire, C., Ganzeveld, L., Gayler, V., van den Hurk, B. J. J. M., Lawrence, P. J., van der Molen, M. K., Müller, C., Reick, C. H., Seneviratne, S. I., Strengers, B. J., and Voldoire, A.: Uncertainties in climate responses to past land cover change: first results from the LUCID intercomparison study, Geophys. Res. Lett., 36, L14814, doi:10.1029/2009GL039076, 2009. 8589
Polcher, J., McAvaney, B., Viterbo, P., Gaertner, M.-A., Hahmann, A., Mahfouf, J.-F., Noilhan, J., Phillips, T., Pitman, A., Schlosser, C., Schulz, J.-P., Timbal, B., Verseghy, D., and Xue, Y.: A proposal for a general interface between land surface schemes and general circulation models, Global Planet. Change, 19, 261–276, doi:10.1016/S0921-8181(98)00052-6, 1998. 8574, 8589
Pothier, D. and Margolis, H.: Analysis of growth and light interception of balsam fir and white birch saplings following precommercial thinning, Ann. For. Sci., 48, 123–132, 1991. 8637
Poulter, B., Ciais, P., Hodson, E., Lischke, H., Maignan, F., Plummer, S., and Zimmermann, N. E.: Plant functional type mapping for earth system models, Geosci. Model Dev., 4, 993–1010, doi:10.5194/gmd-4-993-2011, 2011. 8595
Poulter, B., MacBean, N., Hartley, A., Khlystova, I., Betts, R., Bontemps, S., Brockmann, C., Defourney, P., Hagemann, S., Herold, M., Kirches, G., Lamarche, C., Lederer, D., and Peylin, P.: Plant functional type classification for earth system models: results from the results from the European space agency's land cover climate change initiative, Earth System Science Data, submitted, 2014. 8595, 8600, 8604
Pretzsch, H.: Forest Dynamics, Growth and Yield, Springer-Verlag, Berlin, 2009. 8571, 8598

Pretzsch, H. and Dieler, J.: Evidence of variant intra- and interspecific scaling of tree crown structure and relevance for allometric theory, Oecologia, 169, 637–649, doi:10.1007/s00442-011-2240-5, 2012. 8598, 8638
Quero, J. L., Sterck, F. J., Martínez-Vilalta, J., and Villar, R.: Water-use strategies of six coexisting Mediterranean woody species during a summer drought, Oecologia, 166, 45–57, doi:10.1007/s00442-011-1922-3, 2011. 8639
Reick, C. H., Raddatz, T., Brovkin, V., and Gayler, V.: Representation of natural and anthropogenic land cover change in MPI-ESM, Journal of Advances in Modeling Earth Systems, 5, 459–482, doi:10.1002/jame.20022, 2013. 8569
Reineke, L.: Perfecting a stand-density index for even-aged forests, J. Agric. Res., 46, 627–638, 1933. 8602
Repola, J.: Models for vertical wood density of Scots pine, Norway spruce and birch stems, and their application to determine average wood density, Silva Fenn., 40, 673–685, 2006. 8637
Richards, L. A.: Capillary conduction of liquids through porous mediums, Physica, 1, 318, doi:10.1063/1.1745010, 1931. 8632
Ruimy, A., Dedieu, G., and Saugier, B.: TURC: a diagnostic model of continental gross primary productivity and net primary productivity, Global Biogeochem. Cy., 10, 269–285, doi:10.1029/96GB00349, 1996. 8632
Ryan, M.: The effects of climate change on plant respiration, Ecol. Appl., 1, 157–167, 1991. 8577, 8637
Ryder, J., Polcher, J., Peylin, P., Ottlé, C., Chen, Y., van Gorsel, E., Haverd, V., McGrath, M., Naudts, K., Otto, J., Valade, A., and Luyssaert, S.: A multi-layer land surface energy budget model for implicit coupling with global atmospheric simulations, 2014, in preperation. 8591, 8610
Samuelson, L. J., Stokes, T. A., and Coleman, M. D.: Influence of irrigation and fertilization on transpiration and hydraulic properties of Populus deltoides, Tree Physiol., 27, 765–774, 2007. 8637
Schaaf, C. B., Gao, F., Strahler, A. H., Lucht, W., Li, X., Tsang, T., Strugnell, N. C., Zhang, X., Jin, Y., Muller, J.-P., Lewis, P., Barnsley, M., Hobson, P., Disney, M., Roberts, G., Dunderdale, M., Doll, C., D'Entremont, R. P., Hu, B., Liang, S., Privette, J. L., and Roy, D.: First operational BRDF, albedo nadir reflectance products from MODIS, Remote Sens. Environ., 83, 135–148, doi:10.1016/S0034-4257(02)00091-3, 2002. 8604, 8609

Schäfer, K. V. R., Oren, R., and Tenhunen, J. D.: The effect of tree height on crown level stomatal conductance, Plant Cell Environ., 23, 365–375, 2000. 8637

Schall, P. and Ammer, C.: Can land use intensity be reliably quantified by using a single self-thinning relationship?, Ecol. Appl., 23, 675–677, doi:10.1890/12-0847.1 2013. 8611

Scheiter, S., Langan, L., and Higgins, S. I.: Next-generation dynamic global vegetation models: learning from community ecology, New Phytol., 198, 957–969, doi:10.1111/nph.12210, 2013. 8596

Schulze, E.-D., Cermak, J., Matyssek, R., Penka, M., Zimmerman, R., Vasicek, F., Gries, W., and Kucera, J.: Canopy transpiration and water fluxes in the xylem of the trunk of Larix and Piceu trees – a comparison of xylem flow, porometer and cuvette measurements, Oecologia, 66, 475–483, 1985. 8639

Schulze, E.-D., Schulze, W., Kelliher, F., Vygodskaya, N., Ziegler, W., Kobak, K., Arneth, A., Kusnetsova, W., Sogatchev, A., Issajev, A., Bauer, G., and Hollinger, D.: Abovegound biomass and nitrogen nutrition in a chronosequence of pistine Dahurian Larix stands in eastern Siberia, Can. J. Forest Res., 25, 943–960, 1995. 8637

Sellin, A., Tullus, A., Niglas, A., Õunapuu, E., Karusion, A., and Lõhmus, K.: Humidity-driven changes in growth rate, photosynthetic capacity, hydraulic properties and other functional traits in silver birch (*Betula pendula*), Ecol. Res., 28, 523–535, doi:10.1007/s11284-013-1041-1, 2013. 8639

Shinozaki, K., Yoda, K., Hozumi, K., and Kira, T.: A quantitative analysis of plant form-the pipe model theory: I. Basic analyses, Japanese J. Ecol., 14, 97–105, 1964. 8572, 8577

Simard, M., Pinto, N., Fisher, J. B., and Baccini, A.: Mapping forest canopy height globally with spaceborne lidar, J. Geophys. Res., 116, G04021, doi:10.1029/2011JG001708, 2011. 8604, 8605, 8607, 8612

Simonin, K., Kolb, T. E., Montes-Helu, M., and Koch, G. W.: Restoration thinning and influence of tree size and leaf area to sapwood area ratio on water relations of *Pinus ponderosa*, Tree Physiol., 26, 493–503, doi:10.1093/treephys/26.4.493, 2006. 8578, 8597

Sitch, S., Smith, B., Prentice, I. C., Arneth, A., Bondeau, A., Cramer, W., Kaplan, J. O., Levis, S., Lucht, W., Sykes, M. T., Thonicke, K., and Venevsky, S.: Evaluation of ecosystem dynamics, plant geography and terrestrial carbon cycling in the LPJ dynamic global vegetation model, Glob. Change Biol., 9, 161–185, doi:10.1046/j.1365-2486.2003.00569.x, 2003. 8572, 8577, 8604

Slatyer, R.: Plant–Water Relationships, vol. 158, Academic Press, New York, 1967. 8582

Sperry, J. S., Adler, F. R., Campbell, G. S., and Comstock, J. P.: Limitation of plant water use by rhizosphere and xylem conductance: results from a model, Plant Cell Environ., 21, 347–359, doi:10.1046/j.1365-3040.1998.00287.x, 1998. 8598

Steppe, K., Pauw, D. J. W. D. E., Lemeur, R., and Vanrolleghem, A.: A mathematical model linking tree sap flow dynamics to daily stem diameter fluctuations and radial stem growth, Tree Physiol., 26, 257–273, 2005. 8598

Steudle, E.: Water uptake by plant roots: an integration of views, Plant Soil, 226, 45–56, 2000. 8639

Stöckli, R., Lawrence, D. M., Niu, G.-Y., Oleson, K. W., Thornton, P. E., Yang, Z.-L., Bonan, G. B., Denning, A. S., and Running, S. W.: Use of FLUXNET in the community land model development, J. Geophys. Res., 113, G01025, doi:10.1029/2007JG000562, 2008. 8569

Tarantola, A.: Inverse Problem Theory and Methods for Model Parameter Estimation, SIAM, Philadelpia, 2005. 8597

Thornton, P. E. and Rosenbloom, N. A.: Ecosystem model spin-up: estimating steady state conditions in a coupled terrestrial carbon and nitrogen cycle model, Ecol. Model., 189, 25–48, doi:10.1016/j.ecolmodel.2005.04.008, 2005. 8570

Tyree, M. T. and Sperry, J. S.: Vulnerability of xylem to cavitation and embolism, Annu. Rev. Plant Phys., 40, 19–38, 1989. 8582

Van Genuchten, M.: A closed-form equation for predicting the hydraulic conductivity of unsaturated soils, Soil Sci. Soc. Am., 44, 892–898, 1980. 8583

Verhoef, A. and Egea, G.: Modeling plant transpiration under limited soil water: comparison of different plant soil hydraulic parameterizations and preliminary implications for their use in land surface models, Agr. Forest Meteorol., 191, 22–32, doi:10.1016/j.agrformet.2014.02.009, 2014. 8581

Vicca, S., Luyssaert, S., Peñuelas, J., Campioli, M., Chapin, F. S., Ciais, P., Heinemeyer, A., Högberg, P., Kutsch, W. L., Law, B. E., Malhi, Y., Papale, D., Piao, S. L., Reichstein, M., Schulze, E. D., and Janssens, I.: Fertile forests produce biomass more efficiently, Ecol. Lett., 15, 520–526, doi:10.1111/j.1461-0248.2012.01775.x, 2012. 8597

Vincke, C., Granier, A., Bréda, N., and Devillez, F.: Evapotranspiration of a declining *Quercus robur* (L.) stand from 1999 to 2001. II. Daily actual evapotranspiration and soil water reserve, Ann. For. Sci., 62, 615–623, doi:10.1051/forest:2005060, 2005. 8637

Viovy, N. and de Noblet-Ducoudré, N.: Coupling water and carbon cycle in the biosphere, Sci. Geol. Bull., 50, 109–121, 1997. 8570

Weatherly, P.: Water uptake and flow in roots, Encyclopedia of plant physiology, edited by: Lange, O., Nobel, P. S., Osmond, D., and Ziegler, H., 79–109, Berlin, Springer, 1982.

Whitehead, D.: Regulation of stomatal conductance and transpiration in forest canopies, Tree Physiol., 18, 633–644, doi:10.1093/treephys/18.8-9.633, 1998. 8582

Widlowski, J.-L., Pinty, B., Clerici, M., Dai, Y., De Kauwe, M., de Ridder, K., Kallel, A., Kobayashi, H., Lavergne, T., Ni-Meister, W., Olchev, A., Quaife, T., Wang, S., Yang, W., Yang, Y., and Yuan, H.: RAMI4PILPS: an intercomparison of formulations for the partitioning of solar radiation in land surface models, J. Geophys. Res., 116, G02019, doi:10.1029/2010JG001511, 2011. 8608

Wolf, A., Ciais, P., Bellassen, V., Delbart, N., Field, C. B., and Berry, J. A.: Forest biomass allometry in global land surface models, Global Biogeochem. Cy., 25, GB3015, doi:10.1029/2010GB003917, 2011. 8611

Wullschleger, S. D., Meinzer, F. C., and Vertessy, R. A.: A review of whole-plant water use studies in trees, Tree Physiol., 18, 499–512, 1998. 8637

Xia, J. Y., Luo, Y. Q., Wang, Y.-P., Weng, E. S., and Hararuk, O.: A semi-analytical solution to accelerate spin-up of a coupled carbon and nitrogen land model to steady state, Geosci. Model Dev., 5, 1259–1271, doi:10.5194/gmd-5-1259-2012, 2012. 8570, 8571

Yang, Z., Dickinson, R., Robock, A., and Vinnikov, K.: Validation of the snow submodel of the biosphere – atmosphere transfer scheme with Russian snow cover and meteorological observational data, J. Climate, 10, 353–373, 1997. 8574

Yin, X. and Struik, P.: C3 and C4 photosynthesis models: an overview from the perspective of crop modelling, NJAS-Wagen. J. Life Sc., 57, 27–38, doi:10.1016/j.njas.2009.07.001, 2009. 8575, 8592

Yoda, K., Kira, T., Ogawa, H., and Hozumi, K.: Self-thinning in overcrowded pure stands under cultivated and natural conditions, Journal of the Institute of Polytechnics (Osaka University), 14, 107–129, 1963. 8602

Zaehle, S. and Friend, A. D.: Carbon and nitrogen cycle dynamics in the O-CN land surface model: 1. Model description, site-scale evaluation, and sensitivity to parameter estimates, Global Biogeochem. Cy., 24, GB1005, doi:10.1029/2009GB003521, 2010. 8577, 8604, 8605

Zhao, K. and Jackson, R. B.: Biophysical forcings of land-use changes from potential forestry activities in North America, Ecol. Monogr., 84, 329–353, doi:10.1890/12-1705.1, 2014. 8568

Table 1. Concise description of the modules in the standard ORCHIDEE version with the motivation to change the modules in ORCHIDEE-CAN.

Module	Description	Motivation for change
Albedo	For each PFT the total albedo for the grid square is computed as a weighted average of the vegetation albedo, the soil albedo, and the snow albedo.	The scheme overlooks the effect of vegetation shading bare soil for sparse canopies and gives the ground in all PFTs the same reflectance properties as bare soil.
Soil hydrology	Vertical water flow in the soil is based on the Fokker–Planck equation that resolves water diffusion in non-saturated conditions from the Richards equation (Richards, 1931). The 4 m soil column consists of eleven moisture layers with an exponentially increasing depth (D'Orgeval et al., 2008).	No change
Soil temperature	The soil temperature is computed according to the Fourier equation using a finite difference implicit scheme with seven numerical nodes unevenly distributed between 0 and 5.5 m (Hourdin, 1992).	No change
Energy budget	The coupled energy balance scheme, and its exchange with the atmosphere, is based on that of Dufresne and Ghattas (2001). The surface is described as a single layer that includes both the soil surface and any vegetation.	A big leaf approach does not account for within canopy transport of carbon, water and energy. Further, it is inconsistent with the current multilayer photosynthesis approach and the new multilayer albedo approach.
Photosynthesis	C3 and C4 photosynthesis is calculated following Farquhar et al. (1980) and Collatz et al. (1992), respectively. Photosynthesis assigns artificial LAI levels to calculate the carbon assimilation of the canopy. These levels allow for a saturation of photosynthesis with LAI, but have no physical meaning.	The scheme uses a simple Beer's law transmission of light to each level, which is inconsistent with the albedo scheme.
Autotrophic respiration	Autotrophic respiration distinguishes maintenance and growth respiration. Maintenance respiration occurs in living plant compartments and is a function of temperature, biomass and, the prescribed carbon/nitrogen ratio of each tissue (Ruimy et al., 1996). A prescribed fraction of 28 % of the photosynthates allocated to growth is used in growth respiration (McCree, 1974). The remaining assimilates are distributed among the various plant organs using an allocation scheme based on resource limitations (see allocation).	No change

Table 1. Continued.

Module	Description	Motivation for change
Carbon allocation	Carbon is allocated to the plant following resource limitations Friedlingstein et al. (1999). Plants allocate carbon to their different tissues in response to external limitations of water, light and nitrogen availability. When the ratios of these limitations are out of bounds, prescribed allocation factors are used.	The resource limitation approach requires capping LAI at a predefined value. Due to this cap, the allocation rules are most often not applied, reducing the scheme to prescribing allocation.
Phenology	At the end of each day, the model checks whether the conditions for leaf onset are satisfied. The PFT-specific conditions are based on long and short term warmth and/or moisture conditions (Botta et al., 2000).	No change
Mortality and turnover	All biomass pools have a turnover time. Living biomass is transferred to the litter pool, litter is decomposed or transferred to the soil pool.	This approach is not capable of modelling stand dimensions.
Soil and litter carbon and heterotrophic respiration	Following (Parton et al., 1988), prescribed fractions of the different plant components go to the metabolic and structural litter pools following senescence, turnover or mortality. The decay of metabolic and structural litter is controlled by temperature and soil or litter humidity. For structural litter, its lignin content also influences the decay rate.	No change
Forest management	An explicit distribution of individual trees (Bellassen et al., 2010) is the basis for a process-based simulation of mortality. The aboveground "stand-scale" wood increment is distributed on a yearly time step among individual trees according to the rule of (Deleuze et al., 2004): the basal area of each individual tree grows proportionally to its circumference.	The concept of the original implementation were retained, however, the implementation was adjusted for consistency with the new allocation scheme and to have a larger diversity of management strategies.

Table 2. Variable description. Variables were grouped as follows: F = flux, f = fraction, M = pool, m = modulator, d = stand dimension, T = temperature, p = pressure, R = resistance, q = humidity, g = function.

Symbol in text	Unit	Symbol in ORCHIDEE-CAN	Description
F_{rm}	$gC\,m^{-2}\,s^{-1}$	resp_maint	Maintenance respiration
F_{rg}	$gC\,m^{-2}\,s^{-1}$	resp_growth	Growth respiration
$F_{LW,i}$	$W\,m^{2}$	r_lw	Long wave radiation incident at vegetation level "i"
$F_{SW,i}$	$W\,m^{2}$	r_sw	Short wave radiation incident at vegetation level "i"
F_{trs}	$m\,s^{-1}$	Transpir_supply	Amount of water that a tree can get up from the soil to its leaves for transpiration
$T_{a,i}$	K	temp_atmos_pres, temp_atmos_next	Atmospheric temperature at the "present" and "next" time step, respectively, at level "i"
$T_{L,i}$	K	temp_leaf_pres	Leaf temperature at level "i"
$q_{a,i}$	$kg\,kg^{-1}$	q_atmos_pres, q_atmos_next	Specific humidity at the "present" and "next" time step, respectively, at level "i"
$q_{L,i}$	$kg\,kg^{-1}$	q_leaf_pres	Leaf specific humidity at level "i"
M_l	$gC\,plant^{-1}$	Cl	Leaf mass of an individual plant
M_s	$gC\,plant^{-1}$	Cs	Sapwood mass of an individual plant
M_h	$gC\,plant^{-1}$	Ch	Heartwood mass of an individual plant
M_r	$gC\,plant^{-1}$	Cr	Root mass of an individual plant
M_{linc}	$gC\,plant^{-1}$	Cl_inc	Increment in leaf mass of an individual plant
M_{sinc}	$gC\,plant^{-1}$	Cs_inc	Increment in sapwood mass of an individual plant
M_{rinc}	$gC\,plant^{-1}$	Cr_inc	Increment in root mass of an individual plant
M_{totinc}	gC	b_inc_tot	Total biomass increment
M_{inc}	$gC\,plant^{-1}$	b_inc	Increment in plant biomass of an individual plant
M_{swc}	$m^{3}\,m^{-3}$	swc	Volumetric soil water content
m_w	–	wstress_fac	Modulator for water stress as experienced by the plants
m_ψ	MPa	psi_soil_tune	Modulator to account for resistance in the soil-root interface
m_{Ndeath}	–	scale_factor	Normalization factor for mortality
$m_{LAIcorr}$	–	lai_correction_factor	Adjustable parameter in the calculation of gap probabilities of grasses and crops
d_h	m	height	Plant height
d_l	m^{-2}	–	One sided leaf area of an individual plant

Table 2. Continued.

Symbol in text	Unit	Symbol in ORCHIDEE-CAN	Description
d_s	m^{-2}	–	Sapwood area of an individual plant
d_{hinc}	m	delta_height	Height increment
d_{dbh}	m	dia	Plant diameter
d_{ba}	$m^2\,plant^{-1}$	ba	Basal area
d_{bainc}	$m^2\,plant^{-1}$	delta_ba	Basal area increment
d_{circ}	m	circ	Circumference of an individual plant
d_{ind}	trees	n_circ_class	Number of trees in diameter class /
d_c	m^2	crown_shadow_h	Projected area of an opaque tree crown
d_{csa}	m^2	csa_sap	Projected crown surface area
d_{LAI}	$m^2_{leaf}\,m^{-2}_{ground}$	–	Leaf area index
d_{LAIeff}	–	laieff	Effective leaf area index
$d_{LAIabove}$	–	lai_sum	Sum of the LAI of all levels above the current level
$d_{A,i}$	m^2	–	Cross-sectional area of vegetation level "*i*"
$d_{hi,i}$	m	delta_h	Vegetation height of level "*i*"
$d_{V,i}$	m^3	–	Volume of vegetation level "*i*"
d_{rd}	–	root_dens	Root density
d_λ	ind m^2	–	Inverse of the individual plant density
p_{delta}	MPa	delta_P	Pressure difference between leaves and soil
$p_{\psi sr}$	MPa	psi_soilroot	Bulk soil water potential in the rooing zone
$p_{\psi s}$	MPa	psi_soil	Soil water potential for each soil layer
R_r	MPa s m^{-3}	R_root	Hydraulic resistance of roots
R_{sap}	MPa s m^{-3}	R_sap	Hydraulic resistance of sapwood
R_l	MPa s m^{-3}	R_leaf	Hydraulic resistance of leaves
R_{temp}	MPa s m^{-3}	–	Hydraulic resistance of roots, sapwood or leaves adjusted for temperature
$R_{a,i}$	s m^{-1}	big_r	Aerodynamic resistance of vegetation at level "*i*" in the canopy
$R_{s,i}$	s m^{-1}	big_r_prime	Stomatal resistance of vegetation at level "*i*" in the canopy

Table 2. Continued.

Symbol in text	Unit	Symbol in ORCHIDEE-CAN	Description
f_{Pwc}	–	Pwc_h	Porosity of a tree crown
f^{trees}_{Pgap}	–	PgapL	Gap probability for trees
f^{gc}_{Pgap}	–	PgapL	Gap probability for grasses and crops
f^{bs}_{Pgap}	–	PgapL	Gap probability for bare soil
f^{clar}_{death}	–	mortality	Mortality fraction per circumference class
f_{KF}	–	KF	Leaf allocation factor
f_{LF}	–	LF	Root allocation factor
f_γ	–	gamma	Slope of the intra-specific competition
f_s	m	s	Slope of linearised relationship between height and basal area
f_{rl}	–	leaf_reflectance	Reflectance of a single leaf
f_{tl}	–	leaf_transmittance	Transmittance of a single leaf
f_{Rbgd}	–	bdg_reflectance	Reflectance of the ground beneath the canopy
$f^{f_n}_{Coll,veg}$	–	Collim_alb_BB, Isotrop_alb_BB	Reflected fraction of light to the atmosphere which has collided with canopy elements, separated for direct and diffuse sources, respectively
$f^{f_n}_{UnColl,\,bgd}$	–	Collim_alb_BC, Isotrop_alb_BC	Reflected fraction of light to the atmosphere which has not collided with any canopy elements, separated for direct and diffuse sources, respectively
$f^{T}_{UnColl,\,veg}$	–	Collim_Tran_Uncoll	Transmitted fraction of light to the ground which has not collided with any canopy elements
$f^{f_n}_{Coll,\,bgd,1}$	–	–	Reflected fraction of light which has struck the background a single time and has collided with vegetation
$f^{f_n}_{Coll,\,bgd,n}$	–	–	Reflected fraction of light which has struck the background multiple times and has collided with vegetation
z	m	z_array	Height above the soil
θ_z	radians	solar_angle	Solar zenith angle
θ_μ	radians	–	Cosine of the solar zenith angle
g_G	–	–	Leaf orientation function
g_σ	–	sigmas	Cut-off circumference of the intra-specific competition, calculated as a function of k_{ncirc}

Table 3. Description of the parameters in ORCHIDEE-CAN.

Symbol in text	Unit	Value	Symbol in ORCHIDEE-CAN	Description	References
k_{cmaint}	–	Table 3	coeff_maint_init	Fraction of allocatable photosynthates that is consumed for maintenance and growth respiration	Ryan (1991)
k_{ls}, k_{lsmin}, k_{lsmax}	m	Table 3	k_latosa, k_latosa_min, k_latosa_max	Leaf area to sapwood area of an individual tree	Pothier and Margolis (1991); Bartelink (1997); Berthier et al. (2001); Mencuccini and Bonosi (2001); Wullschleger et al. (1998); Novick et al. (2009); Schäfer et al. (2000); Samuelson et al. (2007); Gould and Harrington (2008); McDowell et al. (2002); Meadows and Hodges (2002); David et al. (2004); Limousin et al. (2012); Bréda and Granier (1996); Martin et al. (1998); Vincke et al. (2005); Margolis et al. (1995)
k_{sar}	–	Eq. (7)	c0_alloc	Sapwood mass to root mass for an individual tree	Calculated from other parameters
k_{Vcmax}	µmol m^{-2} s^{-1}	Table 4	Vcmax25	Carboxylation capacity	TRY
$k_{Jmax/Vcmax}$	µmol e^{-}(µmol CO_2)$^{-1}$	Table 4	arjv	Ratio of electron transport capacity to carboxylation capacity	TRY
k_{sla}	m^2 gC^{-1}	Table 4	sla	Specific leaf mass	TRY
k_{ps}	gC m^{-3}	Table 3	pipe_density	Carbon density of sapwood	TRY; Gaspar et al. (2008); Repola (2006); Knapic et al. (2008); Jenkins et al. (2003)
$k_{\tau l}$	days	Table 3	tau_leaf	Leaf longevity	ICP forest, TRY
$k_{\tau s}$	days	Table 3	tau_sap	Sapwood longevity	Björklund (1999); Longuetaud et al. (2006); Gebauer et al. (2008); Schulze et al. (1995)

Table 3. Continued.

Symbol in text	Unit	Value	Symbol in ORCHIDEE-CAN	Description	References
$k_{\tau r}$	days	Table 3	tau_root	Root longevity	Brunner et al. (2013)
k_{ap}	m	Table 3	pipe_tune1	Parameter in the relationship between diameter and projected crown surface area	Pretzsch and Dieler (2012)
k_{bp}	–	Table 3	pipe_tune_exp_coeff	Parameter in the relationship between diameter and projected crown surface area	Pretzsch and Dieler (2012)
k_{ncirc}	–	3	ncirc	Number of circumference classes	Assumed
$k_{\alpha'}$, $k_{\alpha''}$	n.a.	n.a.	n.a.	Generic parameter to develop Eq. (40)	n.a.
k_{β}	n.a.	n.a.	n.a.	Generic parameter to develop Eq. (40)	n.a.
$k_{\alpha 1}$	m^{-1}	Table 3	pipe_tune2	Allometric constant relating tree diameter and height	Swedish, German, French and Spanish NFI
$k_{\beta 1}$	–	Table 3	pipe_tune3	Allometric constant relating tree diameter and height	Swedish, German, French and Spanish NFI
$k_{\alpha 2}$	–	Table 3	alpha_self_thinning	Allometric constant of the self-thinning relationship	Swedish, German, French and Spanish NFI
$k_{\beta 2}$	–	Table 3	beta_self_thinning	Allometric constant of the self-thinning relationship	Swedish, German, French and Spanish NFI
k_m	–	1	m	Relaxation constant of intra-specific competition relationship	Assumed
k_{ddf}	–	1	death_df	Factor by which the smallest and largest circumference classes differ	Assumed
$k_{\tau_{resid}}$	years	Table 3	residence_time	Residence time of tree, accounting for mortality due to pest, diseases and windfall	Assumed

Table 3. Continued.

Symbol in text	Unit	Value	Symbol in ORCHIDEE-CAN	Description	References
k_{lcon}	m s^{-1} MPa^{-1}	Table 4	k_leaf	Hydraulic conductivity of leaves	Hickler et al. (2006); Sellin et al. (2013); Aranda et al. (2005);
k_{scon}	m^2 s^{-1} MPa^{-1}	Table 4	k_sap	Hydraulic conductivity of sapwood	Manzoni et al. (2013); Cochard (1992): Magnani et al. (2000); Quero et al. (2011); Sellin et al. (2013)
k_{rcon}	m^3 kg^{-1} s^{-1} MPa^{-1}	Table 4	k_root	Hydraulic conductivity of roots	Magnani et al. (2000); Steudle (2000); Arneth et al. (1996)
$k_{\psi 50}$	MPa	Table 4	psi_50	Soil water potential that causes 50 % loss of xlem conductivit through cavitation	Choat et al. (2012); Manzoni et al. (2013); Corcuera et al. (2004); Fichot et al. (2010, 2011); Hickler et al. (2006); Cochard (1992)
$k_{\psi lmin}$	MPa	Table 4	psi_leaf	Minimal leaf water potenial	Choat et al. (2012); Martinez-Vilalta et al. (2004); Magnani et al. (2000); Limousin et al. (2012)l; Hacke and Sauter (1995); Sellin et al. (2013); Schulze et al. (1985)
k_c	–	3	c_cavitation	Shape parameter for vulnerability curve for cavitation	Hickler et al. (2006)
$k_{\alpha 1v}$	–	0.556	a_viscosity(1)	Empirical parameter for the temperature dependence of hydraulic resistance	Cochard et al. (2000)
$k_{\alpha 2v}$	–	0.022	a_viscosity(2)	Empirical parameter for the temperature dependence of hydraulic resistance	Cochard et al. (2000)
$k_{\lambda,LE}$	J kg^{-1}		chalev0	Latent heat of evaporation	
$k_{pa,i}$	kg m^{-3}		rau	Air density, calculated from air temperature and pressure	
$k_{pv,i}$	kg m^{-3}	1000	rho_veg	Leaf density, assumed to be equal to the heat capacity of water	

Table 3. Continuation of Table 3. Soil parameters are given for each soil tile: BS, bare soil, GC: grasses and crops, T: trees.

Symbol in text	Unit	Value	Symbol in ORCHIDEE-CAN	Description	References
$k_{lhc,i}$	J kg K^{-1}	4.1810^{-3}	jtheta	Leaf layer heat capacity	
k_{pw}	g cm^{-3}		rho_h2o	Density of water at 15 °C	
k_g	m s^{-2}		cte_grav	Gravitational constant	
$k_{k,i}$	m^2 s^{-1}	k_eddy	Diffusivity coefficient		
k_{av}	m^{-1}	0.0075 (BS), 0.0036 (GC), 0.0019 (T)	avan_fao	Van Genuchten (1980) coefficient α	Carsel and Parrish (1988)
k_{swcs}	m^3 m^{-3}	0.41 (BS), 0.43 (GC), 0.41 (T)	mcs_fao	Saturated soil water content	Carsel and Parrish (1988)
k_{swcr}	m^3 m^{-3}	0.065 (BS), 0.078 (GC), 0.095 (T)	mcr_fao	Residual soil water content	Carsel and Parrish (1988)
k_{mv}	–	Calculated from n	–	Van Genuchten (1980) coefficient m	Carsel and Parrish (1988)
k_{nv}	–	1.89 (BS), 1.56 (GC), 1.31 (T)	nvan_fao	Van Genuchten (1980) coefficient n	Carsel and Parrish (1988)
$Leaf_{ssa}^{vis}$	–	Table 6	leaf_ssa_vis	Leaf single scattering albedo, visible light	Derived from Pinty et al. (2007)
$Leaf_{ssa}^{nir}$	–	Table 6	leaf_ssa_nir	leaf single scattering albedo, near infrared	Derived from Pinty et al. (2007)
$Leaf_{psd}^{vis}$	–	Table 6	leaf_psd_vis	Leaf preferred scattering direction, visible light	Derived from Pinty et al. (2007)
$Leaf_{psd}^{nir}$	–	Table 6	leaf_psd_nir	Leaf preferred scattering direction, near infrared	Derived from Pinty et al. (2007)
$Bgrd_{ref}^{vis}$	–	Table 6	bgd_reflectance_vis	Background reflectance, visible light	Derived from Pinty et al. (2007)
$Bgrd_{ref}^{vis}$	–	Table 6	bgd_reflectance_nir	Background reflectance, near infrared	Derived from Pinty et al. (2007)

Table 4. Parameter values per species group for allocation and mortality. Te, Temperate; Bo, Boreal; Ne, Needleleaf; Br, Broadleaved; E, Evergreen; S, Summergreen.

MTC	Species (PFT)	k_{cmaint}	k_{lsmin}	k_{lsmax}	k_{ap}	k_{bp}	$k_{\tau l}$	$k_{\tau s}$	$k_{\tau r}$	k_{ps}	$k_{\alpha 1}$	$k_{\beta 1}$	$k_{\alpha 2}$	$k_{\beta 2}$	k_{resid}
TeNeE	*Pinus sylvestris*	0.0330	1100	1395	97	1.47	720	13 870	224	200 000	33	0.63	1236	−0.57	250
TeNeE	*Pinus pinaster*	0.0175	250	1745	54	1.05	1670	15 148	275	235 000	29	0.53	1626	−0.59	250
TeNeE	*Picea sp.*	0.0379	1350	3900	113	0.85	1460	16 425	326	190 000	35	0.54	1507	−0.59	250
TeBrE	*Quercus ilex/suber*	0.0291	675	3079	146	1.52	677	11 680	191	480 000	14	0.33	1678	−0.64	250
TeBrS	*Betula sp.*	0.0097	2600	3600	91	1.16	146	11 680	280	238 000	35	0.66	1272	−0.61	200
TeBrS	*Fagus sylvatica*	0.0130	2700	4430	173	1.70	183	11 680	280	334 000	32	0.52	1000	−0.60	200
TeBrS	*Quercus robur/petraea*	0.0021	3300	4380	173	1.70	183	11 680	280	300 000	32	0.52	1100	−0.60	200
TeBrS	*Populus sp.*	0.0160	5000	5100	139	1.40	183	11 680	280	176 000	39	0.50	1407	−0.60	200
BoNeE	*Pinus sylvestris*	0.0346	2600	4300	70	1.49	1160	11 680	224	200 000	41	0.59	991	−0.58	350
BoNeE	*Picea sp.*	0.0467	2500	3000	40	1.11	2160	11 680	368	190 000	45	0.57	1166	−0.58	350
BoBrS	*Betula sp.*	0.0767	4800	5000	77	1.21	146	11 680	280	238 000	41	0.66	1272	−0.60	150
BoNeS	*Larix sp.*	0.1100	5000	6000	83	1.40	180	13 870	360	248 750	30	0.52	1426	−0.60	350

Table 5. Parameter values per species group for hydraulic architecture and photosynthesis. Te, Temperate; Bo, Boreal; Ne, Needleleaf; Br, Broadleaved; E, Evergreen; S, Summergreen.

MTC	Species (PFT)	k_{lcon}	k_{scon}	k_{rcon}	$k_{\psi 50}$	$k_{\psi lmin}$	k_{Vcmax}	$k_{Jmax/Vcmax}$	k_{sla}
TeNeE	*Pinus sylvestris*	1.50×10^{-7}	8.50×10^{-4}	2.30×10^{-7}	−3.36	−1.60	87	2.48	0.0114
TeNeE	*Pinus pinaster*	1.50×10^{-7}	3.52×10^{-4}	3.30×10^{-7}	−3.22	−2.30	90	1.72	0.005
TeNeE	*Picea sp.*	1.50×10^{-7}	4.00×10^{-4}	4.29×10^{-7}	−3.98	−1.95	61	1.91	0.0072
TeBrE	*Quercus ilex/suber*	1.50×10^{-7}	1.08×10^{-4}	2.56×10^{-6}	−3.83	−4.48	39	2.22	0.0137
TeBrS	*Betula sp.*	3.50×10^{-7}	3.00×10^{-3}	2.51×10^{-7}	−2.40	−0.94	77	2.18	0.0288
TeBrS	*Fagus sylvatica*	3.50×10^{-7}	3.60×10^{-4}	2.01×10^{-7}	−3.98	−2.15	40	2.08	0.0330
TeBrS	*Quercus robur/petraea*	3.50×10^{-7}	1.03×10^{-3}	3.02×10^{-7}	−3.23	−2.94	65	2.04	0.0286
TeBrS	*Populus sp.*	3.50×10^{-7}	1.46×10^{-3}	2.51×10^{-7}	−2.00	−1.62	137	1.40	0.0256
BoNeE	*Pinus sylvestris*	1.50×10^{-7}	8.50×10^{-4}	2.30×10^{-7}	−2.40	−1.60	50	2.48	0.008
BoNeE	*Picea sp.*	1.50×10^{-7}	4.00×10^{-4}	2.45×10^{-7}	−3.20	−1.95	87	2.09	0.0066
BoBrS	*Betula sp.*	3.52×10^{-7}	3.00×10^{-3}	2.51×10^{-7}	−3.15	−0.94	77	2.18	0.0288
BoNeS	*Larix sp.*	2.50×10^{-7}	5.82×10^{-4}	3.00×10^{-7}	−3.66	−1.60	40	2.00	0.0218

Table 6. Parameter values per species group for radiation transfer and photosynthesis. Te, Temperate; Bo, Boreal; Ne, Needleleaf; Br, Broadleaved; E, Evergreen; S, Summergreen.

MTC	Species (PFT)	Leaf_ssa_vis	Leaf_ssa_nir	Leaf_psd_vis	Leaf_psd_nir	Bgrd_ref_vis	Bgrd_ref_nir
TeNeE	*Pinus sylvestris*	0.1529	0.74 131	1.0400	2.1160	0.056 095	0.098 511
TeNeE	*Pinus pinaster*	0.1703	0.78242	1.0946	2.2343	0.058601	0.098511
TeNeE	*Picea sp.*	0.1504	0.74644	1.0395	2.1346	0.042981	0.073559
TeBrE	*Quercus ilex/suber*	0.1343	0.73407	1.0255	2.0953	0.055900	0.095732
TeBrS	*Betula sp.*	0.1722	0.72176	1.0359	2.0575	0.088728	0.14427
TeBrS	*Fagus sylvatica*	0.1415	0.76699	1.0711	2.1959	0.051854	0.089514
TeBrS	*Quercus robur/petraea*	0.1562	0.74554	1.0433	2.1163	0.100240	0.17743
TeBrS	*Populus sp.*	0.1395	0.72523	1.0214	2.0733	0.057965	0.093873
BoNeE	*Pinus sylvestris*	0.1529	0.74131	1.0400	2.1160	0.056095	0.093891
BoNeE	*Picea sp.*	0.1504	0.74644	1.0359	2.1346	0.042981	0.073559
BoBrS	*Betula sp.*	0.1722	0.72176	1.1753	2.0575	0.088728	0.14427
BoNeS	*Larix sp.*	0.1512	0.84980	1.1753	2.4347	0.051740	0.08372

Table 7. Likelihood that the simulated variable comes from the same population as the data. The ORCHIDEE-trunk version does not include effective LAI, basal area and height. Note that the likelihood of Europe (bold) cannot be derived from the values of the other regions due to the overlap between regions.

	ORCHIDEE-CAN							ORCHIDEE-TRUNK						
	GPP	EVAPO	ALB_NIR	ALB_VIS	EFFLAI	BA	HEIGHT	GPP	EVAPO	ALB_NIR	ALB_VIS	EFFLAI	BA	HEIGHT
British Isles	0.91	0.87	0.78	0.45	0.55	0.47	0.13	0.91	0.49	0.74	0.04	–	–	–
Iberian Peninsula	0.80	0.80	0.73	0.65	0.60	0.09	0.66	0.65	0.37	0.25	0.04	–	–	–
France	0.86	0.90	0.92	0.46	0.60	0.66	0.60	0.69	0.46	0.75	0.02	–	–	–
Mid-Europe	0.92	0.93	0.88	0.86	0.68	0.80	0.76	0.81	0.48	0.64	0.46	–	–	–
Scandinavia	0.92	0.83	0.47	0.91	0.59	0.62	0.24	0.81	0.31	0.55	0.65	–	–	–
Alps	0.92	0.86	0.46	0.83	0.68	0.80	0.47	0.77	0.52	0.25	0.52	–	–	–
Mediterranean	0.84	0.77	0.77	0.80	0.65	0.51	0.72	0.54	0.45	0.43	0.45	–	–	–
Eastern Europe	0.93	0.94	0.70	0.93	0.73	0.71	0.76	0.84	0.52	0.51	0.75	–	–	–
Europe	**0.91**	**0.87**	**0.71**	**0.92**	**0.67**	**0.72**	**0.68**	**0.79**	**0.45**	**0.61**	**0.69**	–	–	–

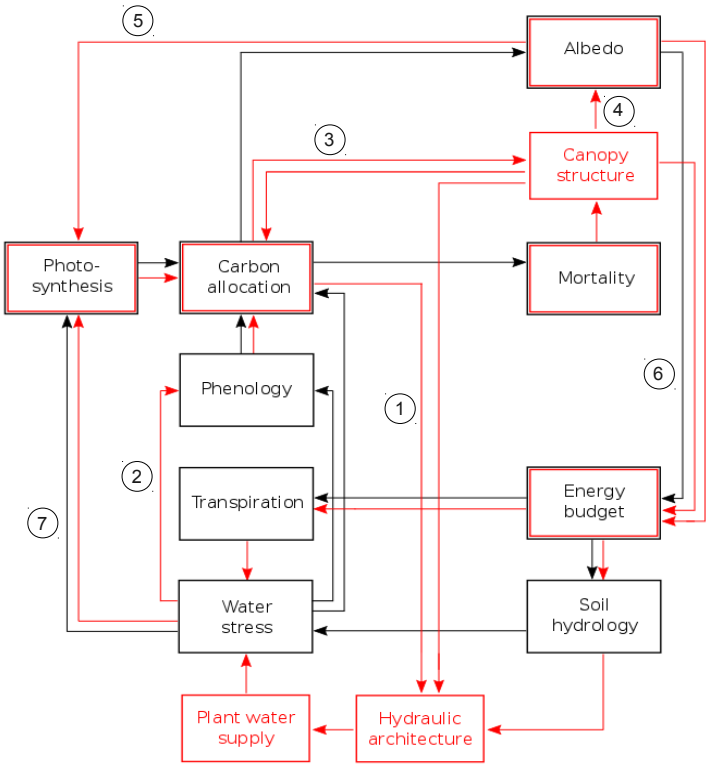

Figure 1. Schematic overview of the changes in ORCHIDEE-CAN. For the trunk the most important processes and connections are indicated in black, while the processes and connections that were added or changed in ORCHIDEE-CAN are indicated in red. Numbered arrows are discussed in Sect. 2.2.

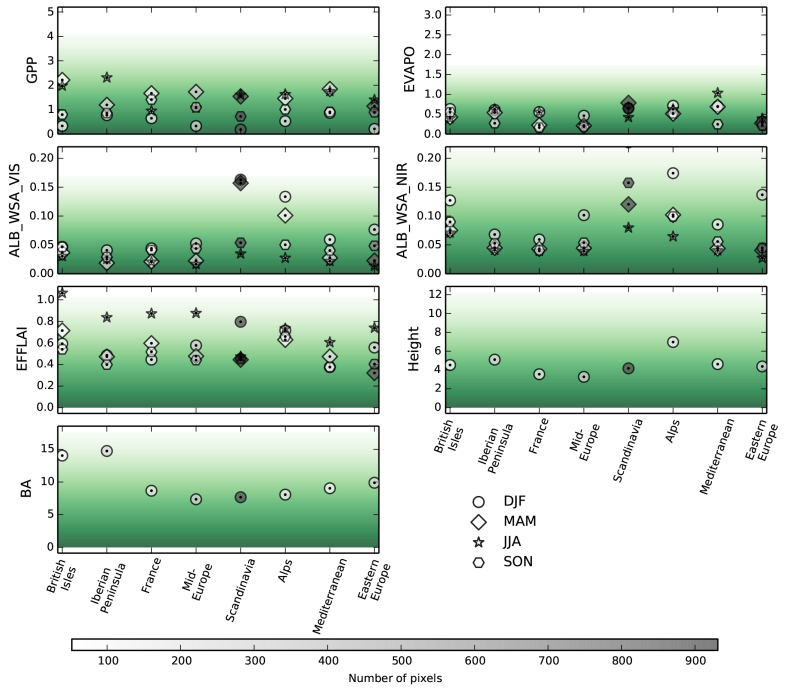

Figure 2. Root mean square error of ORCHIDEE-CAN for gross primary production, evapotranspiration, visible and near-infra-red albedo, effective leaf area index, basal area and height for different regions and periods (DJF: December–February, MAM: March–May, JJA: June–August, SON: September–November). The number of pixels included in the calculation is indicated in a gray-scale. The transition from green to white indicates an RMSE of 100 %.

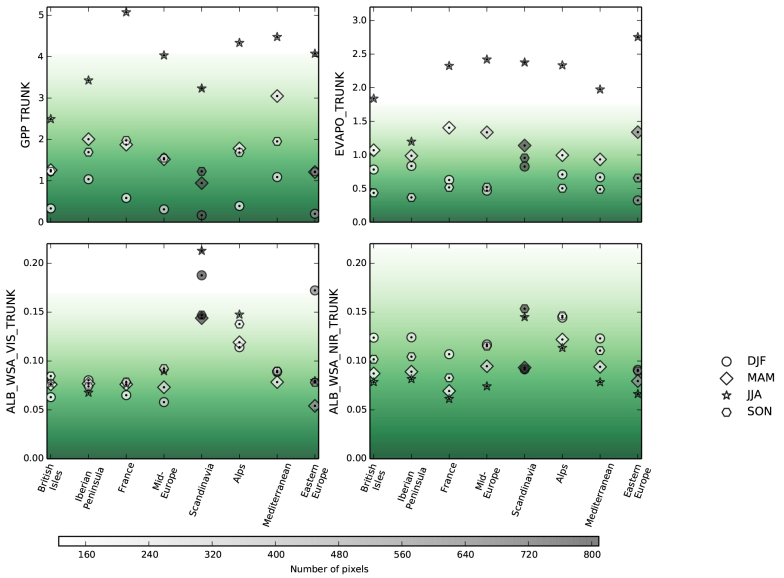

Figure 3. Root mean square error of ORCHIDEE-trunk for gross primary production, evapotranspiration and visible and near-infra-red albedo for different regions and periods (DJF: December–February, MAM: March–May, JJA: June–August, SON: September–November). The number of pixels included in the calculation is indicated in a gray-scale. The transition from green to white indicates an RMSE of 100 %.